Bulletin of the Seismological Society of America, Vol. 98, No. 6, pp. 2694–2714, December 2008, doi: 10.1785/0120080947

Testing Community Velocity Models for Southern California Using the Ambient Seismic Field

by Shuo Ma,* Germán A. Prieto, and Gregory C. Beroza

Abstract We correlate the vertical component of ambient seismic noise data recorded on 56 broadband stations with dense coverage in the greater Los Angeles area to determine station-to-station Green's functions. These Green's functions provide an important test of community velocity models (Southern California Earthquake Center [SCEC] CVM 4.0 and CVM-H 5.2) used for strong ground-motion prediction for future scenario earthquakes in southern California. Comparisons of the ambient-noise Green's functions for nearly 300 paths, with those calculated by the finite-element method in the community velocity models, reveal a strong waveform similarity for the dominant surface waves between 0.1 and 0.2 Hz. We find a mean correlation coefficient between the ambient-noise and finite-element Green's functions of 0.62 for the CVM 4.0 and 0.49 for the CVM-H 5.2, indicating stronger waveform similarity for CVM 4.0. We also find that for 77% of the paths, the surface waves in the finite-element Green's functions for CVM 4.0 arrive early, suggesting that the CVM 4.0 has velocities in the upper 10 km that are too fast along these paths. The same bias is evident for CVM-H 5.2, but is substantially smaller, with only 61% of the paths too fast. For 67% of the paths, CVM 4.0 has velocities faster than CVM-H 5.2. The time lags we obtain between the ambient-noise and finite-element Green's functions provide key information for improving future community velocity models.

Introduction

Seismologists have long recognized that diffuse seismic wave fields, such as the seismic coda and ambient seismic noise, contain useful information about the medium through which they propagate (Aki, 1957; Claerbout, 1968; Aki and Chouet, 1975). The waveforms of the diffuse seismic wave field are, however, difficult to interpret due to both the random distribution of noise sources and scattering from small-scale heterogeneities. Early studies focused on the interpretation of wave intensities (e.g., Sato and Fehler, 1998) while the phase information received less attention (Campillo, 2006).

Wave arrivals between two receivers in a diffuse field, despite their apparent random nature, have a weak coherence that survives multiple scattering. Lobkis and Weaver (2001) and Weaver and Lobkis (2001) showed that correlation of diffuse wave fields recorded at two receivers yields the response of the material recorded at one receiver if there were an impulse excitation at the other receiver (i.e., the Green's function). Early application of correlating diffuse wave fields can be found in helioseismology (Duvall *et al.*, 1993; Rickett and Claerbout, 1999). This concept has also been applied in seismology (e.g., Campillo and Paul, 2003; Shapiro and Campillo, 2004; Paul *et al.*, 2005; Sabra *et al.*, 2005a,b; Shapiro *et al.*, 2005), ultrasonics (e.g., Larose *et al.*, 2004; Malcolm *et al.*, 2004), and ocean acoustics (e.g., Roux *et al.*, 2004; Sabra *et al.*, 2005). It can be extended to other linear systems as well (Snieder *et al.*, 2007).

Theoretical proof of the principle of extracting Green's function by correlating diffuse wave fields has been derived from normal mode theory (Lobkis and Weaver, 2001; Weaver and Lobkis, 2001, 2004), the representation theorem (Wapenaar, 2004), a stationary phase approximation (Snieder, 2004), and plane-wave superposition (Sánchez-Sesma and Campillo, 2006; Sánchez-Sesma *et al.*, 2006). Most derivations assume an isotropic distribution of uncorrelated noise sources and/or scatterers for the true Green's function to be retrieved, a situation that may not be satisfied.

In seismology, Campillo and Paul (2003) and Paul *et al.* (2005) demonstrated that summing correlations of seismic coda over many earthquake sources reveals station-to-station Green's functions. Correlation of ambient seismic noise over long times can also yield station-to-station Green's functions (Shapiro and Campillo, 2004; Sabra *et al.*, 2005a,b; Shapiro *et al.*, 2005). The method works because ambient-noise sources (whether actual sources) or secondary sources (due

*Now at Department of Geological Sciences, San Diego State University, 5500 Campanile Drive, San Diego, California 92182.

to scattering) randomize the wave field over long time periods. The ambient-noise approach exploits the coverage of dense seismic networks without using active sources or waiting for earthquakes to occur. A number of recent studies have used the results from ambient seismic noise correlation to constrain the seismic velocity structure of the Earth (e.g., Sabra *et al.*, 2005a,b; Shapiro *et al.*, 2005; Gerstoft *et al.*, 2006; Yao *et al.*, 2006, 2008; Brenguier *et al.*, 2007; Cho *et al.*, 2007; Lin *et al.*, 2007, 2008; Moschetti *et al.*, 2007; Yang *et al.*, 2007, 2008; Benson *et al.*, 2008; Liang *et al.*, 2008; Zheng *et al.*, 2008) and the Moon (Larose *et al.*, 2005). The ambient seismic noise has also been applied in detecting coseismic velocity changes in the crust (Wegler and Sens-Schönfelder, 2007) and predicting volcanic eruptions (Brenguier *et al.*, 2008) and earthquake ground motions (Prieto and Beroza, 2008).

In this article, we correlate monthly vertical velocity data recorded in January 2007 on 56 broadband seismic stations in southern California with dense coverage of the greater Los Angeles area (Fig. 1) to obtain station-to-station Green's functions that are shown to be stable over the whole year. Using these station-to-station Green's functions, we test two community velocity models developed for southern California (Magistrale *et al.*, 2000; Kohler *et al.*, 2003; Süss and Shaw, 2003) by the Southern California Earthquake Center (SCEC). These velocity models play a central role in large-scale strong ground-motion simulations (e.g., Olsen, *et al.*, 1995; Graves, 1998; Komatitsch *et al.*, 2004; Olsen *et al.*, 2006; Ma *et al.*, 2007). Current versions of the two models are the SCEC CVM 4.0 and CVM-H 5.2 (Fig. 2).

Ambient-noise Green's functions provide an independent and important evaluation of both community velocity

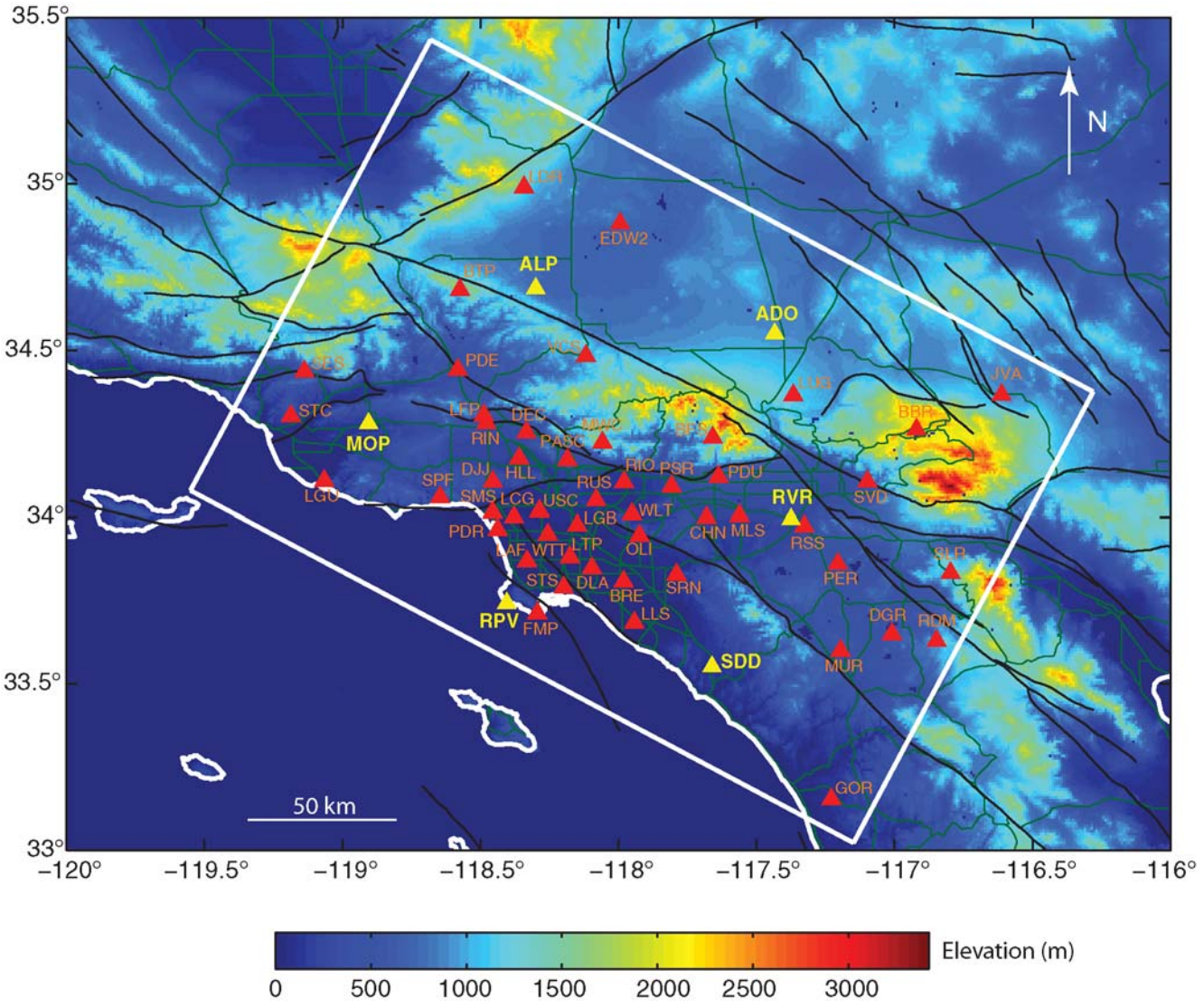

Figure 1. Distribution of the 56 broadband seismic stations (triangles) in southern California used in this study. The six stations in yellow (ADO, ALP, MOP, RPV, SDD, and RVR) are where we correlate data with all the other stations, resulting in ambient-noise Green's functions for 315 ray paths with a good coverage across the Los Angles basin. The white rectangle shows the area we include in the finite-element simulations. Major faults and roads in the area are depicted in black and green lines, respectively.

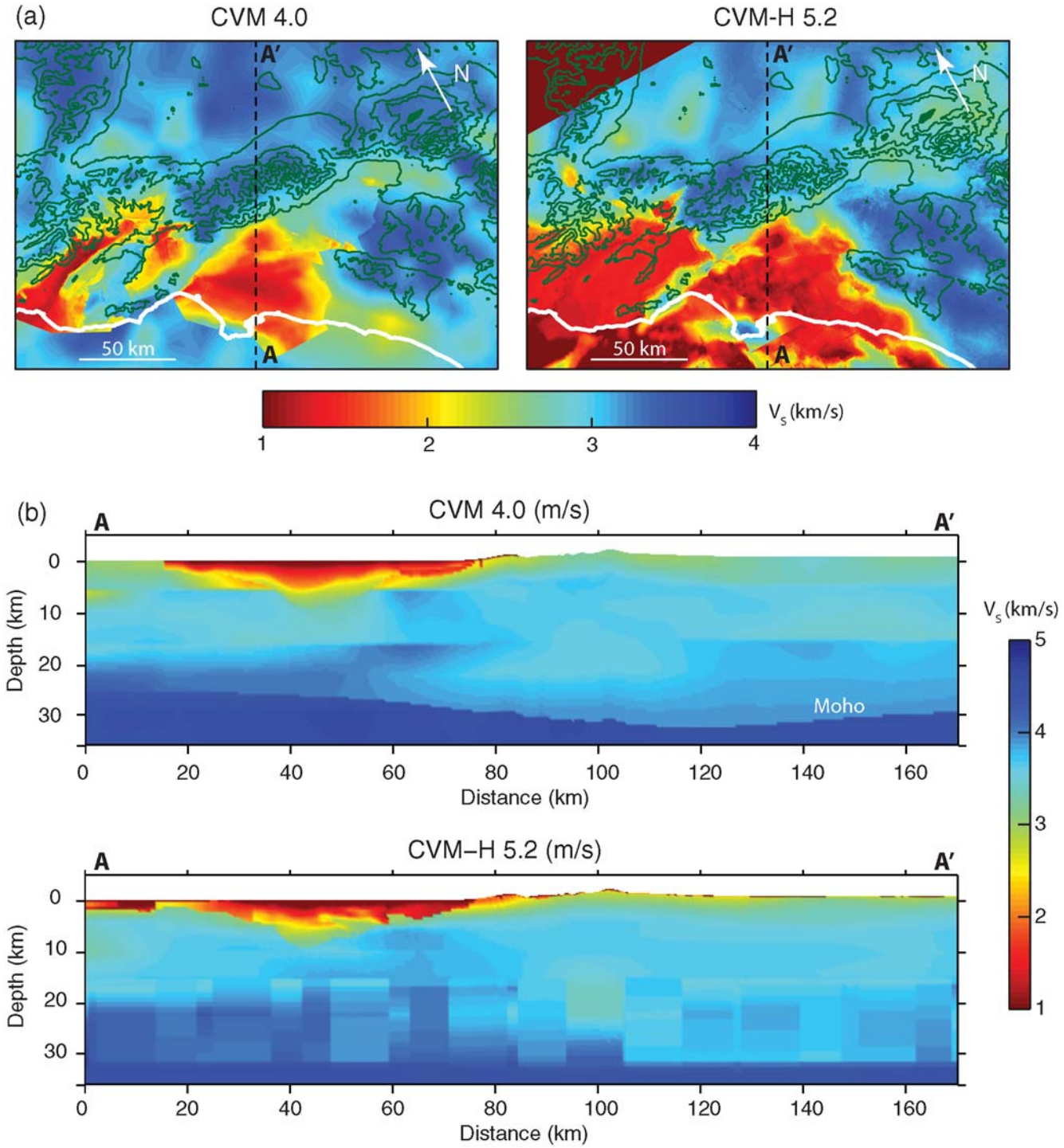

Figure 2. (a) Depth-averaged shear-wave velocity from surface to 3 km below the zero elevation for the CVM 4.0 and CVM-H 5.2 in the area outlined by the white rectangle in Figure 1. The thick white line depicts the coastline. Green contours show surface topography. The CVM-H 5.2 includes the offshore basin structures, while the CVM 4.0 does not. The CVM-H 5.2 has no data coverage in the dark red area on the upper left corner of the right panel. (b) The cross section of the *S*-wave velocity in the CVM 4.0 and CVM-H 5.2 along the dashed line in (a). The CVM-H 5.2 has a finer resolution at shallow depths, especially at the basins. However, the resolution is poorer at large depths. In the regions where the CVM-H 5.2 has no coverage, we use the material properties retrieved from the CVM 4.0 in the finite-element simulations.

models with a coverage that is more complete than that provided by local earthquakes. We test the current community velocity models (CVM 4.0 and CVM-H 5.2) by comparing the ambient-noise Green's functions with theoretical Green's functions calculated by the finite-element method of Ma and Liu (2006). We compute theoretical Green's functions at all 56 stations by applying a vertical force at six stations (ADO, ALP, MOP, RPV, SDD, and RVR) (Fig. 1). This gives

rise to 315 ray paths with good azimuthal coverage across the basins in Los Angeles. Comparisons of the Green's functions along most ray paths show strong waveform similarity for the dominant surface waves in the microseism band (0.1–0.2 Hz), confirming the validity of extracting the Green's function from ambient seismic noise and demonstrating a reasonably good representation of the velocity structure in both community models. We find that CVM 4.0 generates Green's functions that correlate better with the ambient-noise Green's functions than CVM-H 5.2. Accurate time lags between theoretical and observed Green's functions are identified for each ray path, suggesting that both community velocity models have bias. We find surface-wave velocities that are too fast along 77% of the paths for CVM 4.0 and 61% of the paths for CVM-H 5.2.

In the following, we first show the steps for obtaining the Green's functions from ambient-noise correlation. We show that the correlation itself corresponds to the velocity station-to-station Green's function in 3D if the correlation is dominated by narrowband signals. We then describe the finite-element calculation of theoretical Green's functions in CVM 4.0 and CVM-H 5.2. Finally, we compare the Green's functions obtained from the two distinct approaches and evaluate the two community velocity models.

Retrieval of Green's Functions from Ambient Seismic Noise

The 3D displacement Green's function between two receivers is related to the negative time derivative of cross correlation (e.g., Lobkis and Weaver, 2001; Weaver and Lobkis, 2001; Snieder, 2004; Roux *et al.*, 2005, Sabra *et al.*, 2005a,b; Gerstoft *et al.*, 2006; Sánchez-Sesma and Campillo, 2006). The relationship can be written as

$$-\frac{d}{dt}\langle C_{ij}^{\mathrm{disp}}(\mathbf{r}_1,\mathbf{r}_2,t)\rangle \approx G_{ij}^{\mathrm{disp}}(\mathbf{r}_1,\mathbf{r}_2,t) - G_{ij}^{\mathrm{disp}}(\mathbf{r}_1,\mathbf{r}_2,-t), \tag{1}$$

where the Green's function $G_{ij}^{\mathrm{disp}}(\mathbf{r}_1,\mathbf{r}_2,t)$ relates a unit force in direction i at receiver $\mathbf{r}_1$ to the displacement response in direction j at receiver $\mathbf{r}_2$; $\langle\rangle$ denotes the ensemble average—usually taken over a long time span. The correlation $C_{ij}^{\mathrm{disp}}(\mathbf{r}_1,\mathbf{r}_2,t)$ is defined as

$$C_{ij}^{\mathrm{disp}}(\mathbf{r}_1,\mathbf{r}_2,t) = \int_0^T u_i(\mathbf{r}_1,\tau)u_j(\mathbf{r}_2,t+\tau)\,d\tau, \tag{2}$$

where u is the displacement and T is the temporal length of observations. By taking the time derivative of equation (1), it can be shown that the velocity Green's function relates to the correlation as

$$-\frac{d^2}{dt^2}\langle C_{ij}^{\mathrm{disp}}(\mathbf{r}_1,\mathbf{r}_2,t)\rangle \approx G_{ij}^{\mathrm{vel}}(\mathbf{r}_1,\mathbf{r}_2,t) + G_{ij}^{\mathrm{vel}}(\mathbf{r}_1,\mathbf{r}_2,-t). \tag{3}$$

If the cross correlation $\langle C_{ij}^{\mathrm{disp}}(\mathbf{r}_1,\mathbf{r}_2,t)\rangle$ is dominated by a narrowband signal, the property $-\frac{d^2}{dt^2}\langle C_{ij}^{\mathrm{disp}}(\mathbf{r}_1,\mathbf{r}_2,t)\rangle \approx \langle C_{ij}^{\mathrm{disp}}(\mathbf{r}_1,\mathbf{r}_2,t)\rangle$ yields

$$\langle C_{ij}^{\mathrm{disp}}(\mathbf{r}_1,\mathbf{r}_2,t)\rangle \approx G_{ij}^{\mathrm{vel}}(\mathbf{r}_1,\mathbf{r}_2,t) + G_{ij}^{\mathrm{vel}}(\mathbf{r}_1,\mathbf{r}_2,-t). \tag{4}$$

This indicates that the correlation of displacement records at two stations gives rise to the station-to-station velocity Green's function. It can be shown that if the correlation is dominated by narrowband signals, the correlation of displacement, velocity, or acceleration gives nearly identical results. Thus we obtain

$$\langle C_{ij}^{\mathrm{vel}}(\mathbf{r}_1,\mathbf{r}_2,t)\rangle \approx G_{ij}^{\mathrm{vel}}(\mathbf{r}_1,\mathbf{r}_2,t) + G_{ij}^{\mathrm{vel}}(\mathbf{r}_1,\mathbf{r}_2,-t), \tag{5}$$

which indicates that the correlation of velocity records gives the velocity Green's function. This is consistent with the result of Malcolm *et al.* (2004) and Wapenaar (2004). In a 2D space, the cross correlation itself corresponds to the displacement Green's function (Derode *et al.*, 2003; Sánchez-Sesma and Campillo, 2006; Sánchez-Sesma *et al.*, 2006).

In this article, we use equation (5) and correlate velocity records to obtain the station-to-station velocity Green's functions. We selected 56 broadband seismic stations (Fig. 1) in the Southern California Seismic Network (SCSN) that recorded continuous data in January 2007 (see the Data and Resources section). The monthly data (40 samples/sec) are divided into 372 2 hr segments. We chose the 2 hr segment because it is long enough for the coherent signals to propagate between each station pair we study. We removed the mean and trend, and we band-pass filtered each 2 hr segment between 0.01 and 5 Hz before calculating the cross correlation.

Figure 3a details the steps to obtain the Green's function between stations FMP and ADO by cross correlating 2 hr long vertical velocity records. The procedure follows closely that of Benson *et al.* (2007). To remove the effects of earthquakes and local noise sources, we apply sign-bit normalization to the signals. We then apply spectral normalization by whitening the spectra to broaden the frequency range before cross correlation. Clear coherent signals, the desired station-to-station Green's function, show up in the one-month stacks; however, the signal violates the temporal symmetry expected from equation (5). This is because the predominant noise source is from the ocean (closer to FMP than ADO), causing greater coherence for positive time lags. For this reason, we adopt the side of the larger amplitude correlation as the ambient-noise Green's functions. The station-to-station Green's function has dominant energy in a narrow frequency band between 0.1 and 0.2 Hz (Fig. 3a).

Because the noise sources (such as ocean storms) are likely to change with time during a year, we also test the robustness of the Green's function by comparing the correlation of monthly data for four different months and of yearly data (Fig. 3b). For the station pair ADO and FMP, the Green's function for each month shows zero time lag with

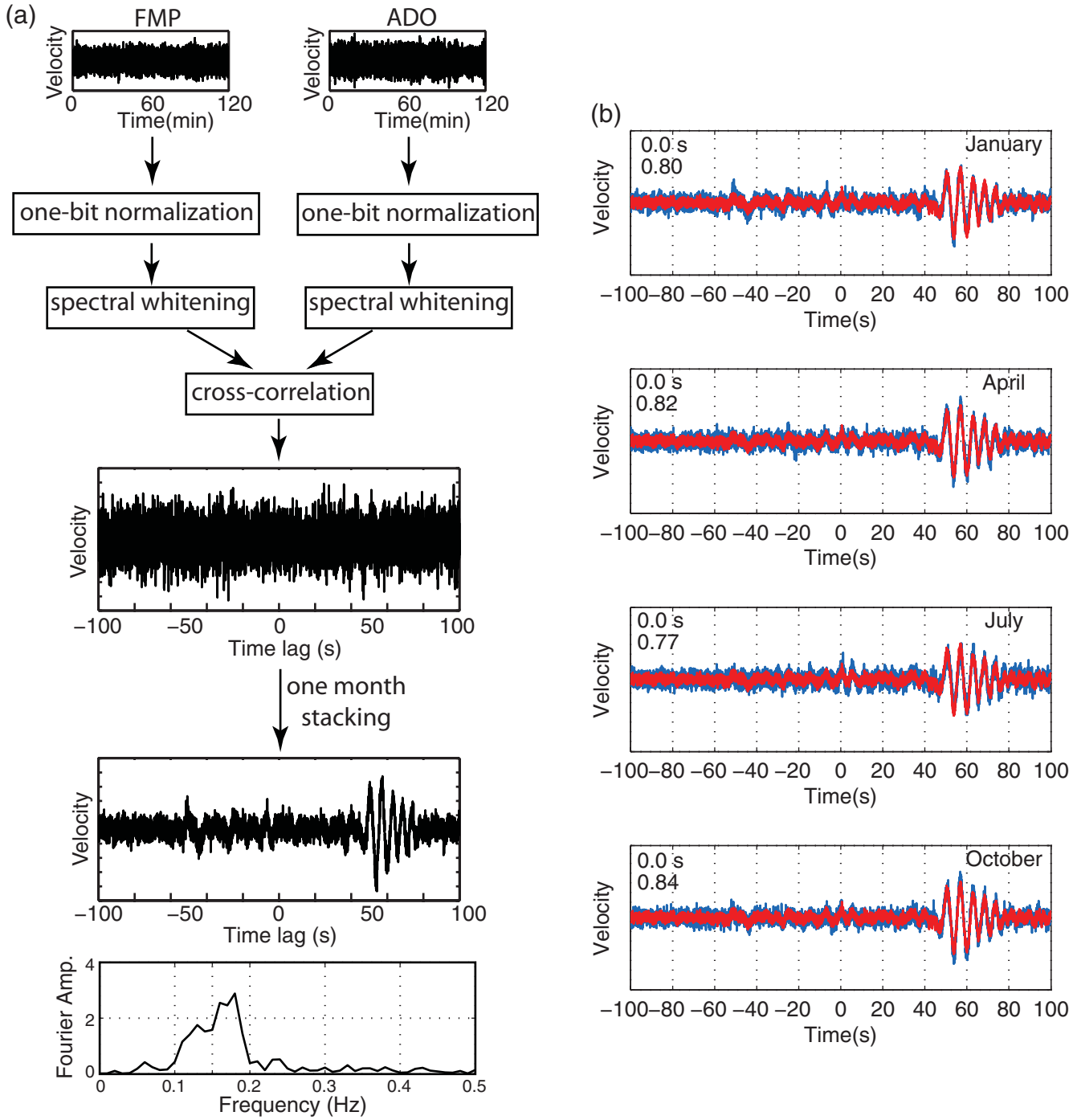

Figure 3. (a) Steps to obtain Green's function between a station pair ADO and FMP from ambient-noise correlation. We calculate cross correlation for 2 hr long velocity time series and stack one month of correlations (372 stacks) to retrieve the station-to-station velocity Green's function. The amplitude spectrum of the Green's function shows that the dominant energy band is between 0.1 and 0.2 Hz. (b) Comparison of Green's function by correlating monthly (blue) and yearly (red) data for the station pair ADO and FMP for four different months in 2007. The time lag and correlation between the two Green's functions are denoted on each panel, showing that the Green's function by correlating monthly data is stable over the whole year.

the Green's function by correlating yearly data, though the 1 yr correlation has a larger signal-to-noise ratio (SNR) in the negative time lags. This illustrates that the correlation of monthly data gives rise to the stable Green's function over the whole year, and it is insensitive to the noise sources. This is the case for all of the station pairs we test with different orientations with respect to the coast.

To demonstrate the technique, we extract all three components of the ambient-noise Green's function at station FMP by correlating the vertical velocity of station ADO with

all three components of velocity at station FMP. The Green's functions correspond to the responses at station FMP due to a vertical unit force at ADO. Figure 4 shows the comparison of all three components at station FMP based on ambient-noise Green's functions and the theoretical finite-element Green's functions calculated using the method of Ma and Liu (2006) by applying a smooth vertical force with Gaussian time dependence [$f(t) = e^{-0.5(t-t_0)^2}$ and $t_0 = 5$ sec] at station ADO in the two community velocity models. The ambient-noise seismograms are obtained by convolving the ambient-noise Green's functions with the force $f(t)$. Because the ambient-noise Green's functions contain dominant energy between 0.1 and 0.2 Hz, we band-pass filtered all of the seismograms in this narrow frequency band. We normalize the amplitude of ambient-noise Green's functions by a common factor such that the vertical response has a unit peak amplitude and the relative amplitudes among the three components are preserved.

The waveforms show remarkable similarity, especially in the north–south and vertical components, indicating the validity of extracting Green's functions from ambient seismic noise and that both CVM 4.0 and CVM-H 5.2 provide a good representation of the velocity structure along this path. The amplitude mismatch in the east–west component, however, suggests that there is room for improvement. Strong waveform similarity allows an accurate time lag to be retrieved between the ambient-noise and finite-element Green's functions. For example, the finite-element seismo-

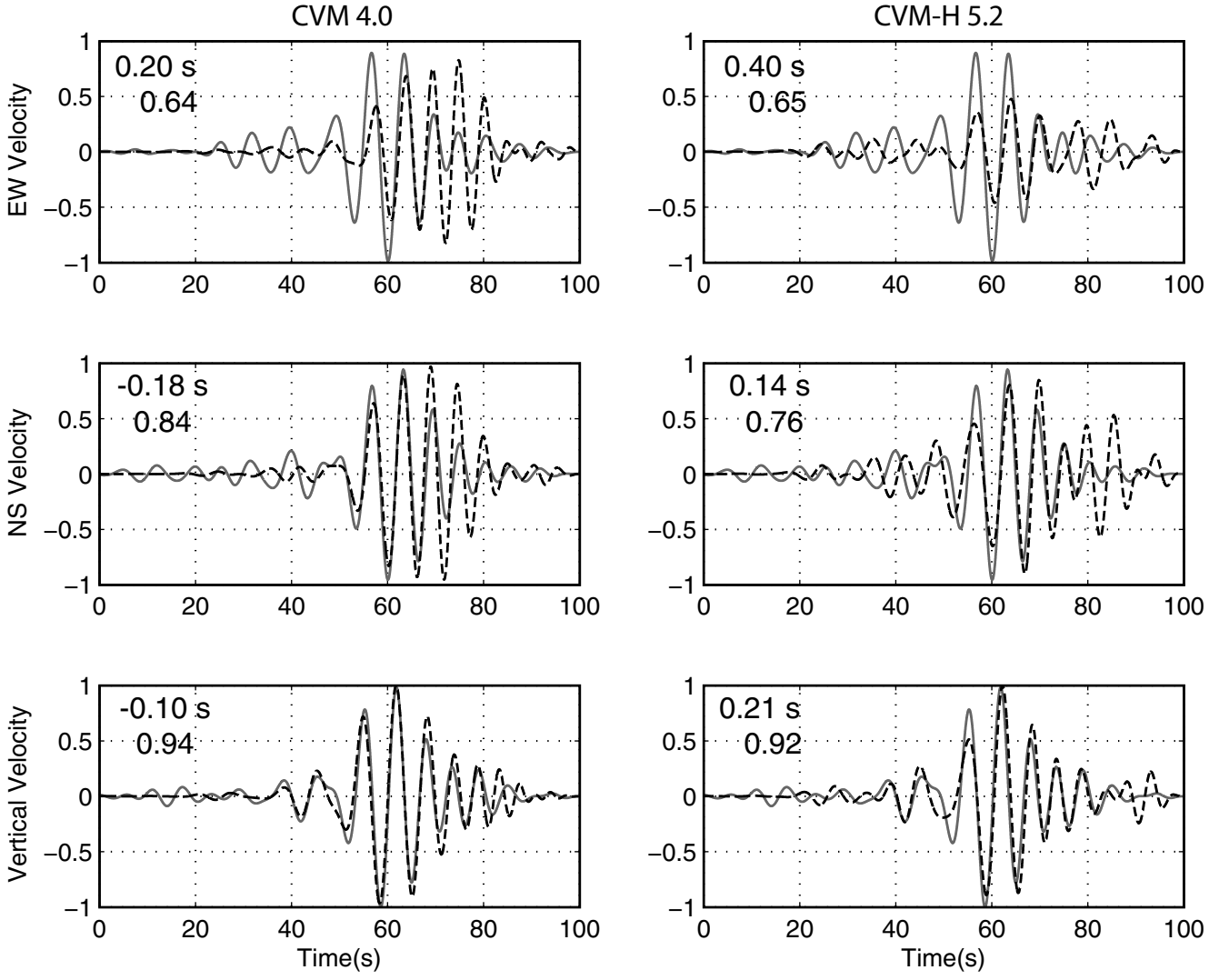

Figure 4. Comparison of the three-component seismograms based on the ambient-noise correlation (gray solid line) and the finite-element seismograms (black dashed line) at station FMP due to a vertical Gaussian force at station ADO. The finite-element seismograms are computed in the CVM 4.0 (left column) and CVM-H 5.2 (right column). All of the seismograms are band-pass filtered between 0.1 and 0.2 Hz. All of the three components are normalized by a common factor such that the vertical component has the unit amplitude. The time lag of the finite-element waveform relative to the noise waveform (positive being that the ambient-noise waveform arrives earlier) and the normalized correlation coefficient between the two waveforms are denoted on each panel.

gram (vertical component) in CVM 4.0 arrives 0.10 sec faster than the ambient-noise seismogram, whereas it is 0.21 sec slower in CVM-H 5.2. Different time lags between the CVM 4.0 and CVM-H 5.2 can also be seen on the other two components. Across the three components in each velocity model, we see a different time lag as well. For example, in the CVM-H 5.2, the time lag for the vertical component is 0.21 sec, whereas it is 0.40 sec for the east–west component and 0.14 sec for the north–south component. This suggests some small anisotropy in the velocity structure. In the following, however, we will test the community velocity models by focusing only on the vertical-to-vertical correlations and leave the correlations with the horizontal components for future work.

We cross correlate the velocities at all 56 stations with the velocity at stations ADO, ALP, MOP, RPV, SDD, and RVR, respectively (Fig. 1). This gives rise to 315 station-to-station Green's functions with good azimuthal coverage in the Los Angeles area, which strongly constrains the velocity structure. Ambient-noise Green's functions show coherent wave propagation, which is dominated by surface waves (Fig. 5). Large variations in the waveforms of Green's functions can be seen along different paths, which is a direct indication of the complex velocity structure of the region.

Calculation of Theoretical Green's Functions in the Community Velocity Models

CVM 4.0 (Magistrale *et al.*, 2000; Kohler *et al.*, 2003) is a 3D rule-based velocity description, where compressional wave velocity (V_P) is defined as a function of sediment age and depth. Several significant stratigraphic horizons are defined, and the velocity within a stratigraphic interval is obtained by vertical interpolation. CVM-H 5.2 (after Süss and Shaw, 2003) is a V_P model based on tens of thousands of direct velocity measurements taken from well logs, seismic reflection data, and geostatistical interpolation techniques that take into account the lateral and vertical variations of lithology in the basin. It has a high-resolution model in the Los Angeles basin and a low-resolution model outside of the basin. In both models, shear-wave velocity and density values are defined based on empirical relationships with V_P. Both community velocity models use the tomography model of Hauksson (2000) for regional velocities. The two models differ substantially in their formulation and in their representations of crustal velocity structure in southern California (Fig. 2).

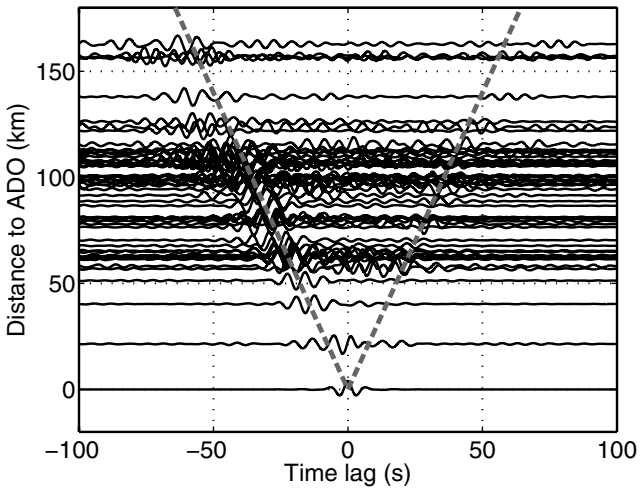

Figure 5. Green's functions from correlation of vertical velocities at all 56 stations with the vertical velocity at station ADO. The Green's functions are band-pass filtered between 0.1 and 0.2 Hz. The gray dashed lines show the move-out of 2.8 km/sec for reference. The complex waveforms indicate the heterogeneity of the underlying velocity structure of the region.

To calculate the theoretical Green's functions, we use a versatile finite-element method (Ma and Liu, 2006) with eight-node hexahedral elements, one-point integration, and hourglass controls. It has been validated in propagating elastic seismic waves in domains of simple geometry (Ma and Liu, 2006) as well as in the presence of surface topography (Ma *et al.*, 2007). It allows easy incorporation of a perfectly matched layer (PML) absorbing boundary and an efficient way of accounting for seismic attenuation (Ma and Liu, 2006).

In the finite-element method, we calculate the station-to-station Green's function as the response to a vertical force applied at the Earth's surface, that is, Lamb's problem (Lamb, 1904). Figure 6 shows the comparison of the finite-element solution with the analytical solution obtained by the Cagniard de Hoop method (de Hoop, 1960) in a homogeneous half-space. Excellent agreement between both solutions demonstrates the accuracy of the finite-element method.

We solve Lamb's problem in the heterogeneous velocity structure described by the community velocity models (CVM 4.0 and CVM-H 5.2) to obtain the theoretical station-to-station Green's functions. Our computational domain covers a large area (250.4 × 170.4 km) of southern California (Fig. 1) and extends to a depth of 36 km below sea level. The four corners of our computational domain are at (−118.681°, 35.433°), (−119.55°, 34.08°), (−117.149°, 33.023°), and (−116.281°, 34.376°). A slightly unstructured mesh is used (see Fig. 7 of Ma and Liu, 2006). The element size is about 100 m in the upper 3 km and reaches 400 m near the bottom, to maintain ~10 nodes per *S*-wave wavelength. This results in a total of about 180 million elements and nodes. The minimum shear-wave velocity in the simulations is 500 m/sec. We simulate waves up to 0.5 Hz. Because of the important effects of surface topography on propagation of surface waves (Ma *et al.*, 2007), we incorporate the surface topography in the simulations. The PML absorbing boundary is used along all of the boundaries of the computational domain except for the free surface. Because both community velocity models do not have anelastic attenuation properties of the velocity structure, we only consider elastic wave effects.

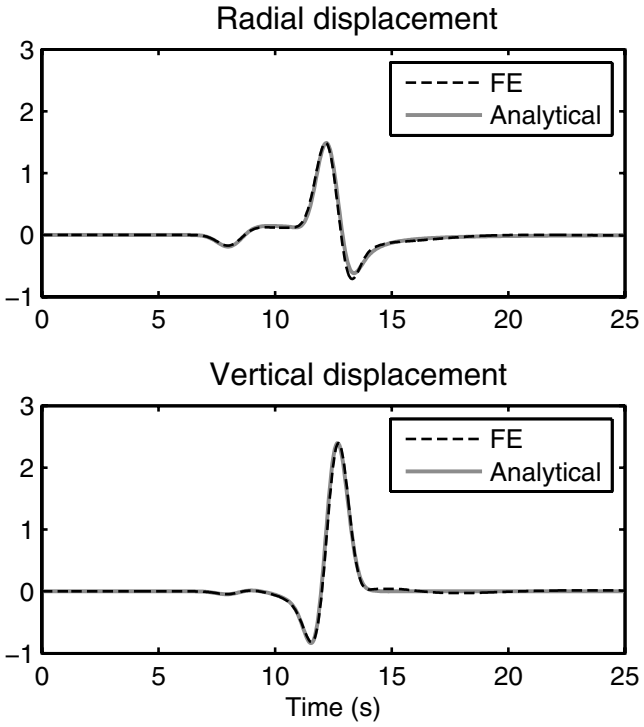

Figure 6. Comparison of the finite-element solution with the analytical solution for the Lamb's problem in a homogeneous half-space ($\rho = 2700$ kg/m^3, $V_P = 6000$ m/sec, and $V_S = 3464$ m/sec) at a point 30 km from the source at the surface. The vertical force at the source has a Gaussian type $f(t) = e^{-2(t-t_0)^2}$, where $t_0 = 3$ sec. The element size in the finite-element simulation is 300 m. Both solutions are low-pass filtered at 1 Hz.

For our six reference stations (ADO, ALP, MOP, RPV, SDD, and RVR) we calculate theoretical Green's functions by applying a vertical force at each, which provides 315 theoretical Green's functions to be compared with the corresponding ambient-noise Green's functions. Figure 7 shows snapshots of vertical velocity response across the whole computational region in both the CVM 4.0 and CVM-H 5.2 due to a force with Gaussian time dependence [$f(t) = e^{-0.5(t-t_0)^2}$ and $t_0 = 5$ sec] at station ADO. The same force is used in all of the finite-element simulations. The wave fields in this simulation correspond to the Green's functions obtained for CVM 4.0 and CVM-H 5.2 convolved with an applied time dependence, $f(t)$. The wavefronts are almost circular in the first 20 sec, indicating a laterally homogeneous velocity structure for the Mojave area in both community models. Excellent absorption of Raleigh waves by the PML is apparent from the lack of edge effects in the simulation. The heterogeneous basin models have a significant effect on wave propagation, as seen at 44 and 56 sec. The different interference patterns of waves in the basin are caused by the large differences between CVM 4.0 and CVM-H 5.2 (Fig. 2).

Results

Figure 8a shows the finite-element Green's functions at all 56 stations due to the force $f(t)$ at station ADO as well as the ambient-noise Green's functions. Because the ambient-noise Green's function contains energy predominantly in the 0.1–0.2 Hz frequency band, we band-pass filtered all of the waveforms between 0.1 and 0.2 Hz. Strong waveform similarity is seen at most stations. The correlation coefficient between the ambient-noise and finite-element Green's functions is shown in each comparison. We see, in general, a better correlation of the finite-element Green's functions in CVM 4.0 with the ambient-noise Green's functions than those in CVM-H 5.2 for these paths.

The strong waveform similarity allows an accurate time-lag measurement between the finite-element and ambient-noise waveforms (Fig. 8a). We obtain the time lag by shifting the finite-element waveform with respect to the ambient-noise waveform to maximize the cross-correlation coefficient. We allow the time-lag to vary between −4 and 4 sec. The observed differences in surface-wave arrival times suggest that both community velocity models have biases. For the paths from ADO, most finite-element waveforms in both velocity models arrive earlier than the ambient-noise waveforms, indicating that both models have material velocities that are too fast for these paths. The mismatch is greater for CVM 4.0, which is slightly faster than CVM-H 5.2 for most of these paths.

Comparisons of waveforms at all 56 stations from ALP, MOP, RPV, SDD, and RPV are shown in Figures 8b,d,e,f. Strong waveform similarity can be seen for most paths, with the time lag between waveforms noted. There are some paths with a poor correlation between the ambient-noise and finite-element Green's functions, such as ADO-LDR and ADO-SMS in both community models and ADO-BRE and ADO-STC in the CVM-H 5.2 (Fig. 8). This mismatch could reflect either a shortcoming of the velocity model and/or the ambient-noise Green's functions.

For similar waveforms, the time lags between the ambient-noise and finite-element seismograms indicate the sense in which the community velocity models might be off. We calculate the time lags between the two but only show the results (Fig. 9) for which the waveforms are sufficiently similar by requiring the correlation coefficient to be above 0.3 and the interstation distance to be larger than 30 km, because the station-to-station Green's functions for shorter distances are likely contaminated by local noise sources. Of the 315 possible paths, these requirements leave 279 paths for CVM 4.0 and 229 paths for CVM-H 5.2. The maps illustrate the paths where the two community velocity models are affected by biases in the material velocities.

We plot the correlation coefficients for all of the ray paths (interstation distance greater than 30 km) as a function of the length and azimuth of the ray path in both community velocity models and the histograms of the correlation coefficient (Fig. 10). We also plot the difference in the correlation coefficient between CVM 4.0 and CVM-H 5.2 for each path. In total, there are 295 ray paths. The azimuth (between 0° and 180°) is defined as the angle from the north rotated clockwise to the ray path. We find that the correlation between

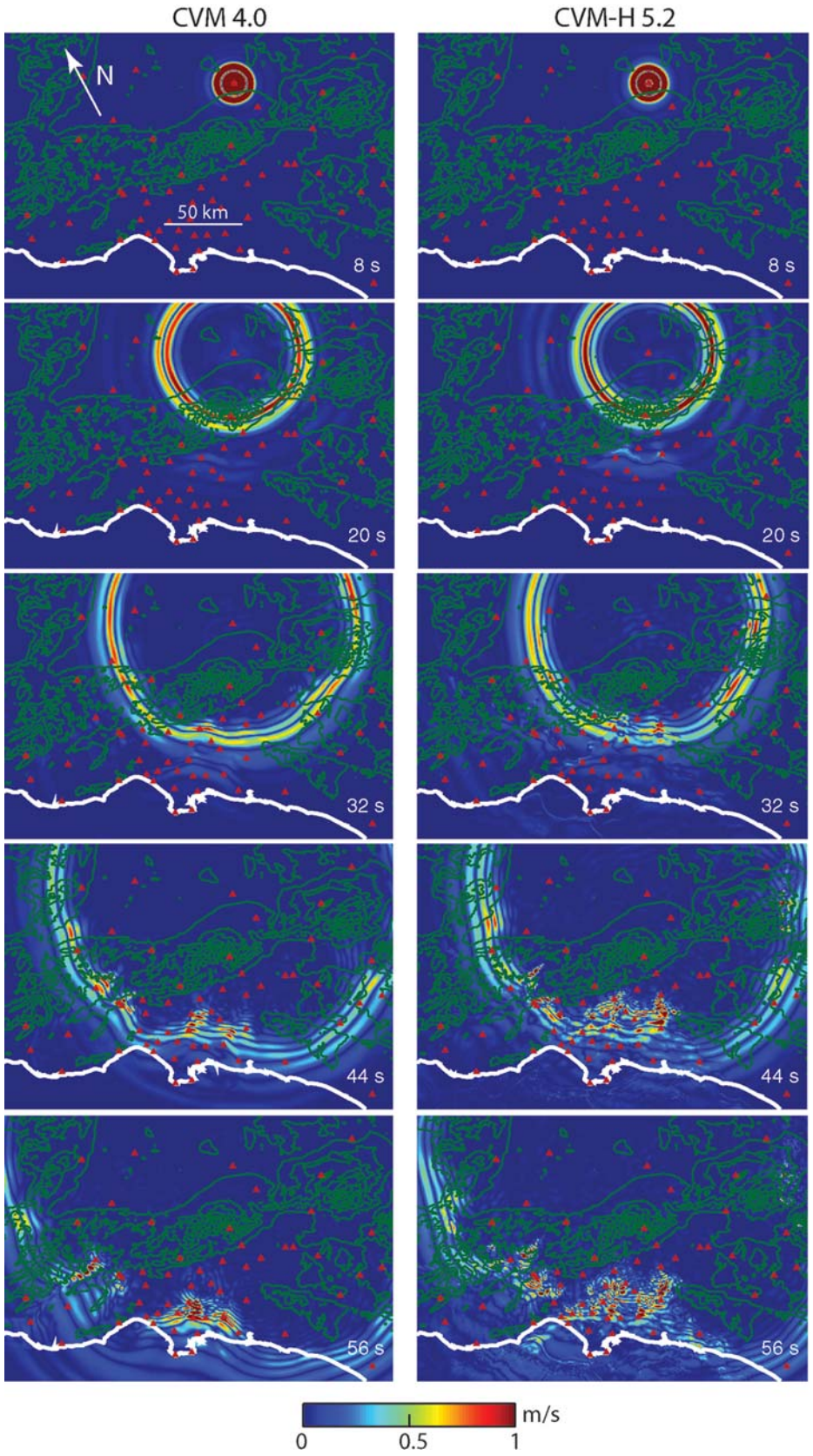

Figure 7. Snapshots of vertical surface velocity (0–0.5 Hz) in the finite-element simulation due to a vertical force at station ADO using the CVM 4.0 and CVM-H 5.2. The green contours show the topography. Stations used in our study are denoted by red triangles. Amplitude scale is saturated to better illustrate features. An excellent absorption of Rayleigh wave is seen by the PML. Large differences in wave fields can be seen in the basins.

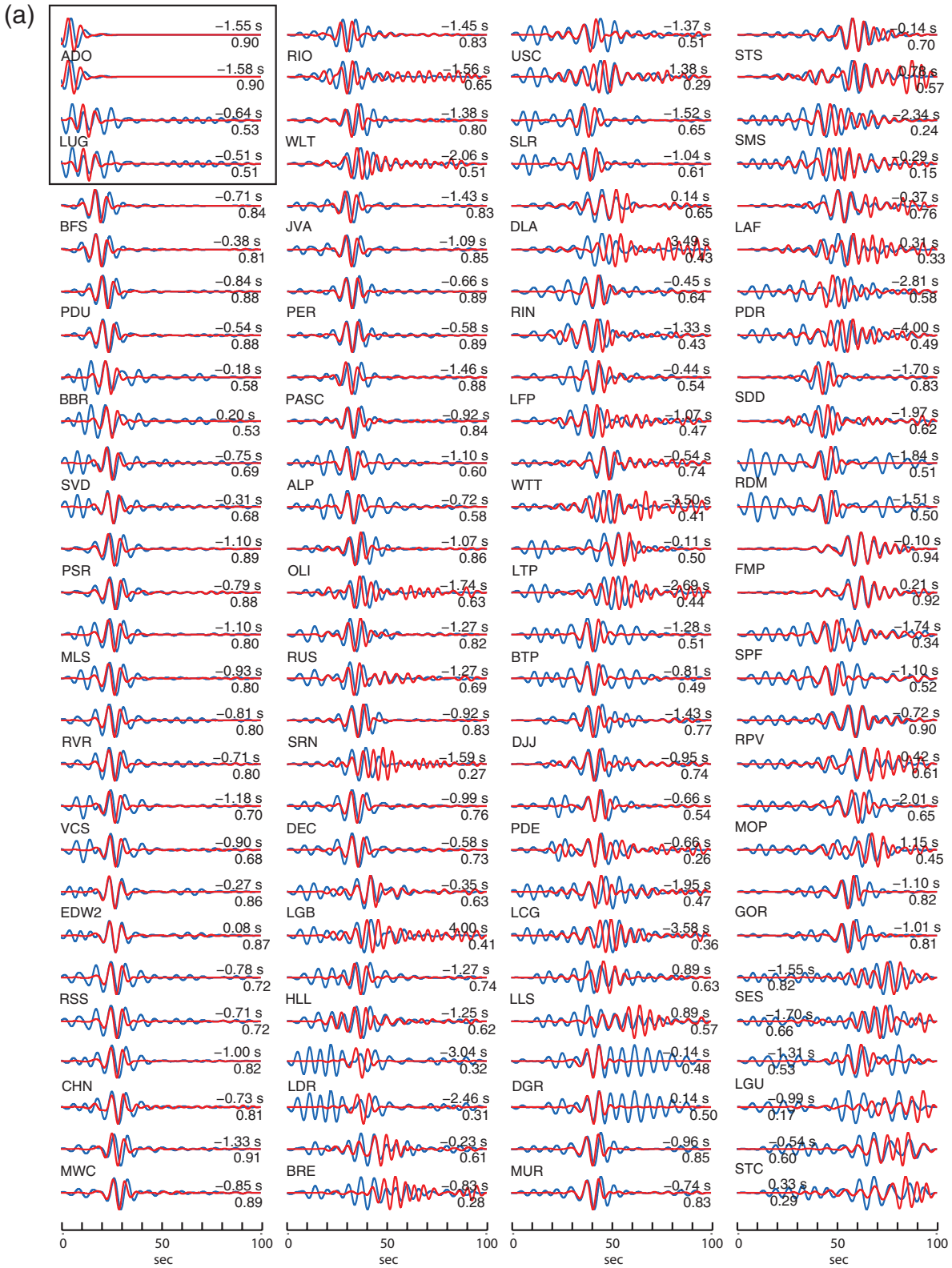

Figure 8. Comparisons of the vertical velocity waveforms using the Green's function from ambient noise (blue) with finite-element seismograms (red) assuming that the virtual source is at station (a) ADO, (b) ALP, (c) MOP, (d) RPV, (e) SDD, and (f) RVR. Both time series are band-pass filtered between 0.1 and 0.2 Hz. Amplitudes are normalized. The first trace for each station uses the CVM 4.0 for the finite-element simulation, while the second trace uses the CVM-H 5.2. The time lag (positive being that the ambient-noise seismogram arrives earlier) and normalized correlation coefficient between the two waveforms are denoted above and below each trace. The stations are sorted by the distance to the virtual source in an ascending order. The black box includes the stations with distance to the virtual source smaller than 30 km, which are excluded in our statistical analyses. (*Continued*)

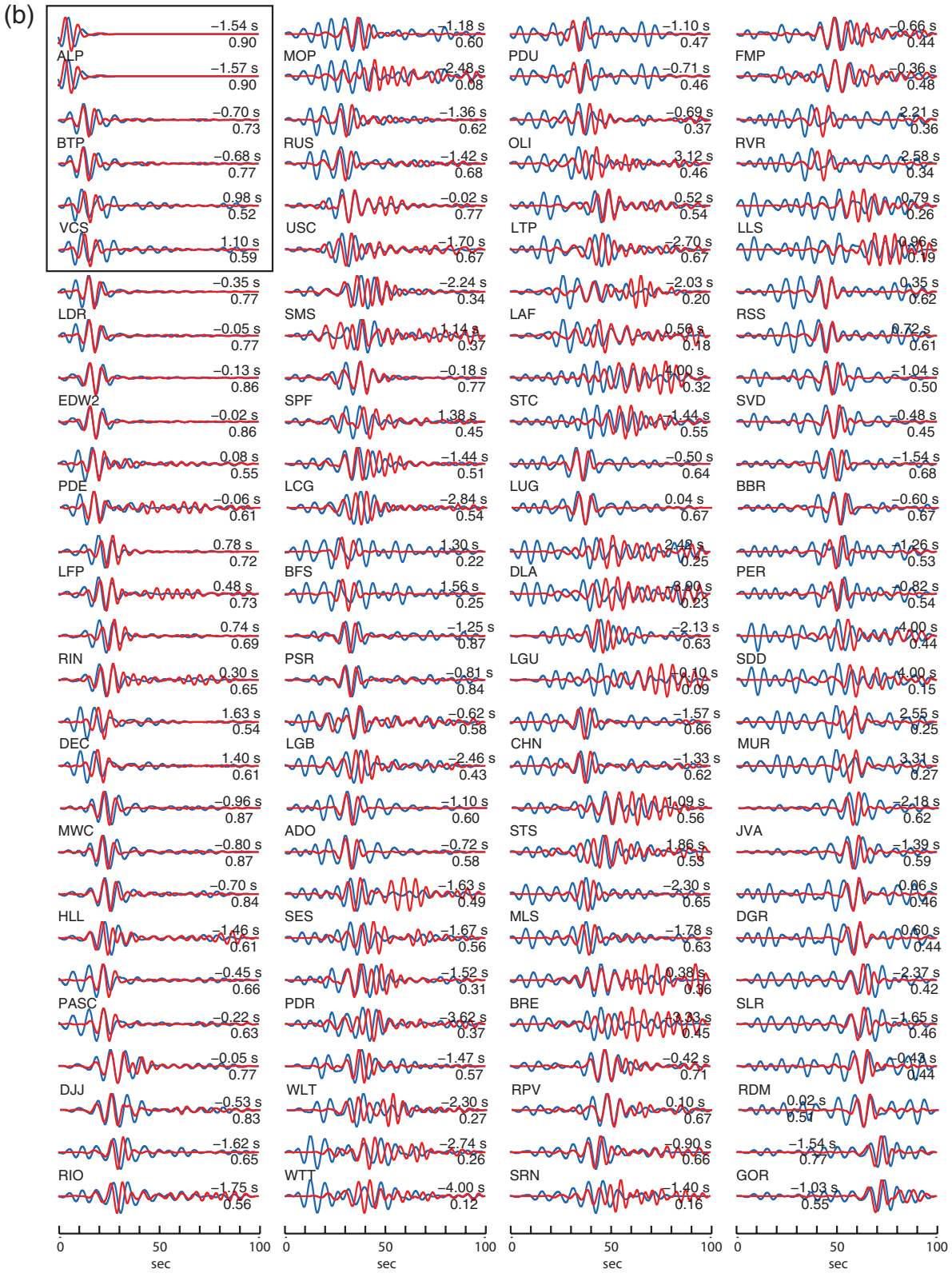

Figure 8. Continued.

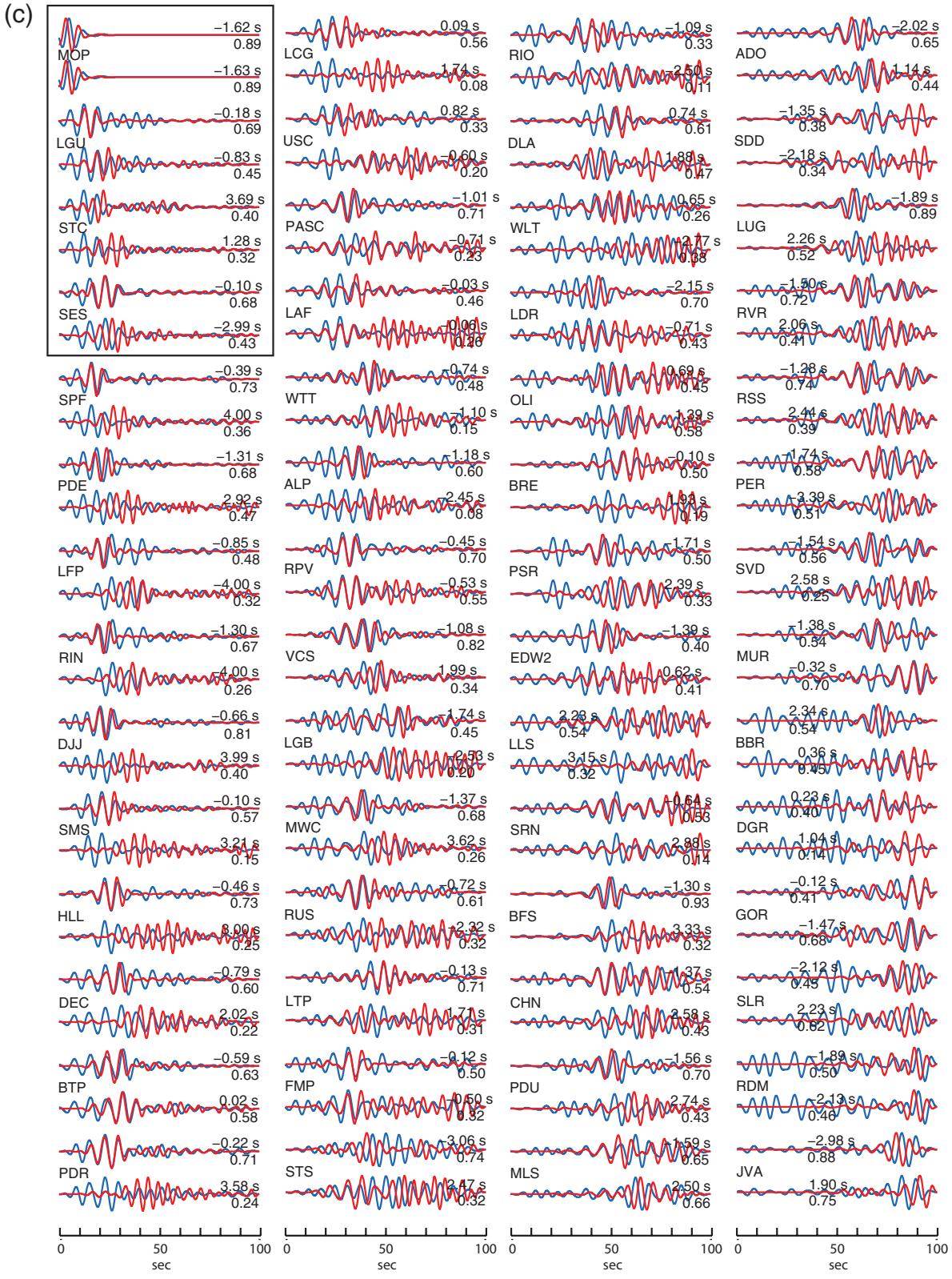

Figure 8. Continued.

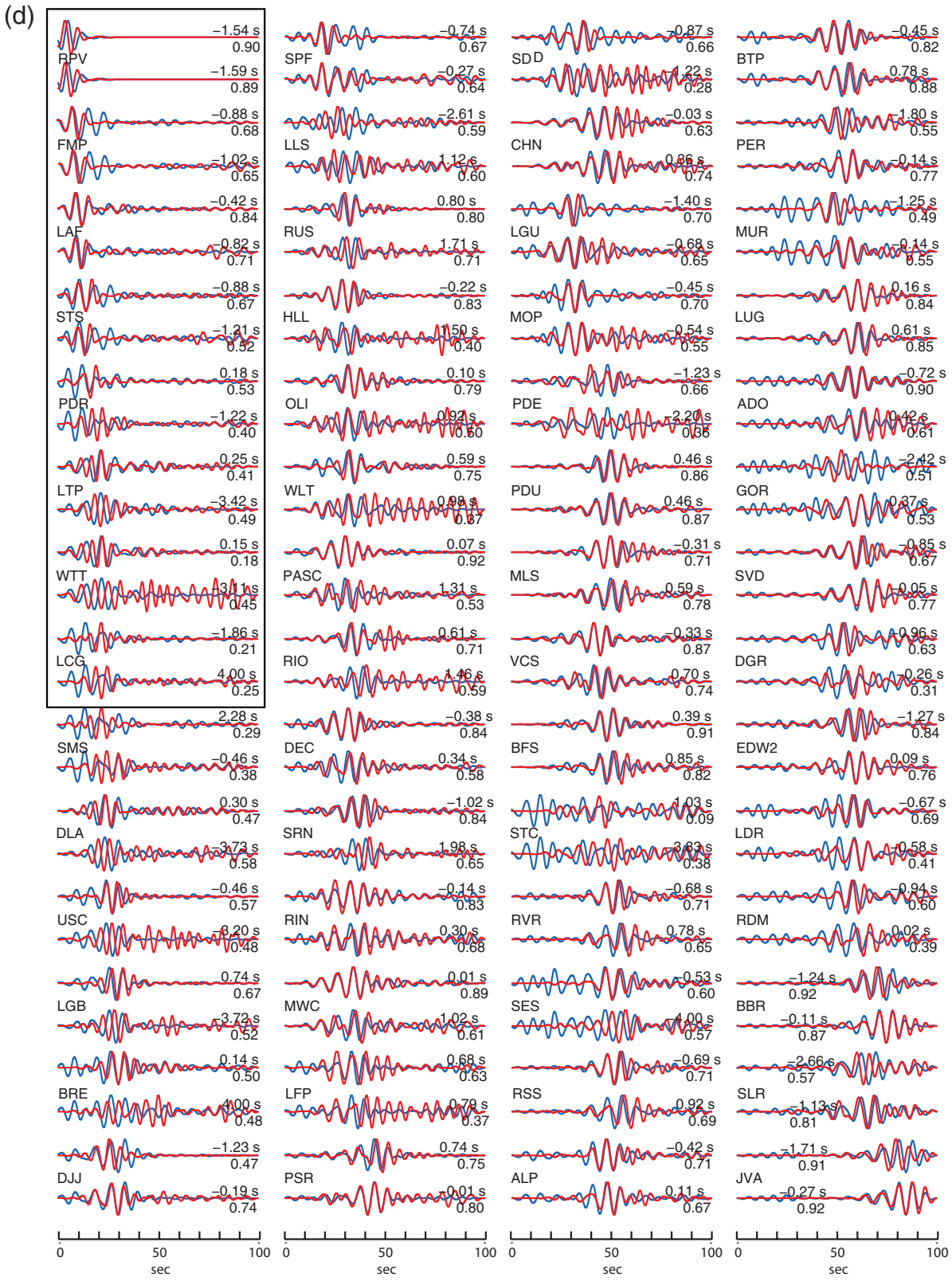

Figure 8. Continued.

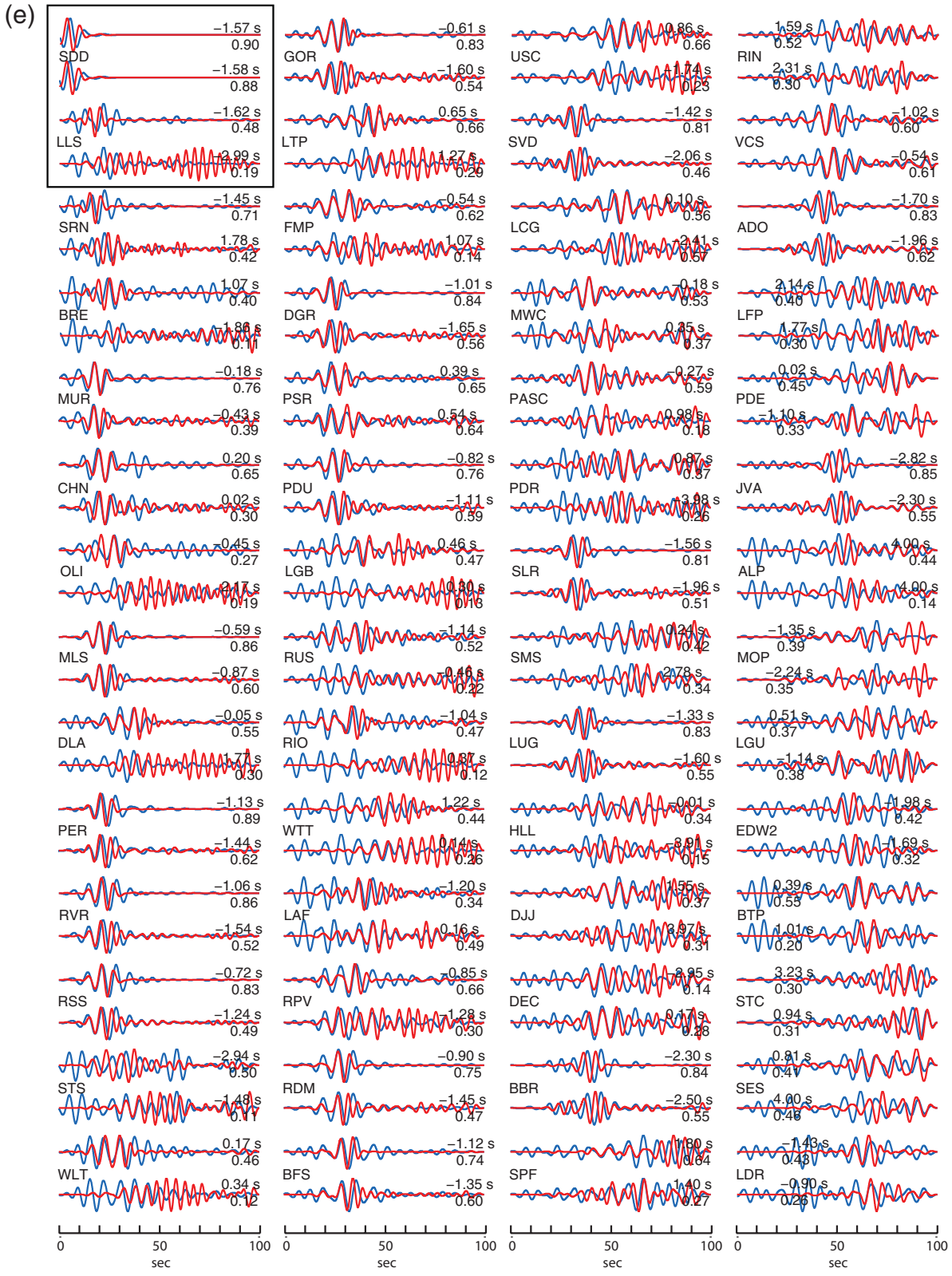

Figure 8. Continued.

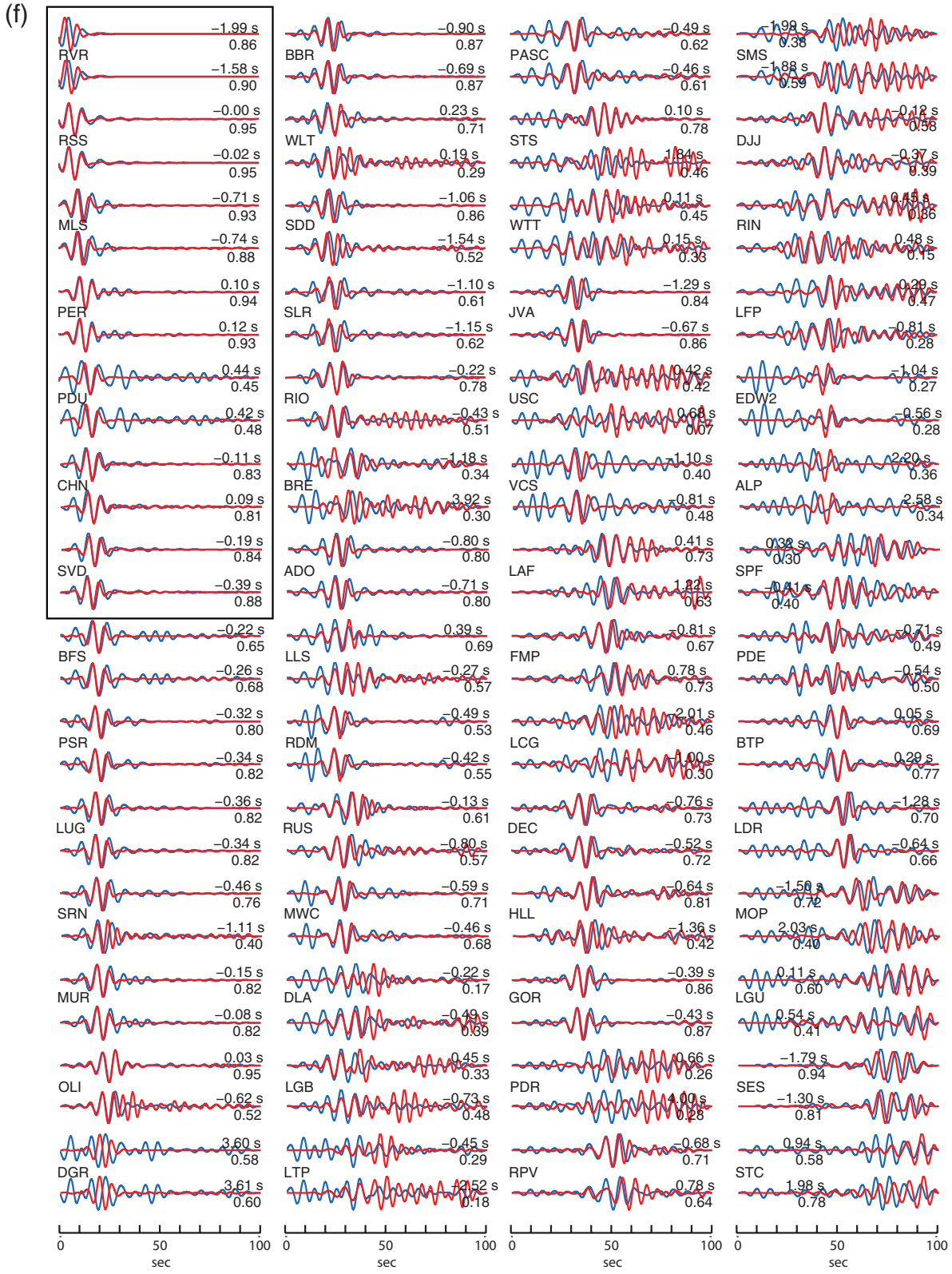

Figure 8. Continued.

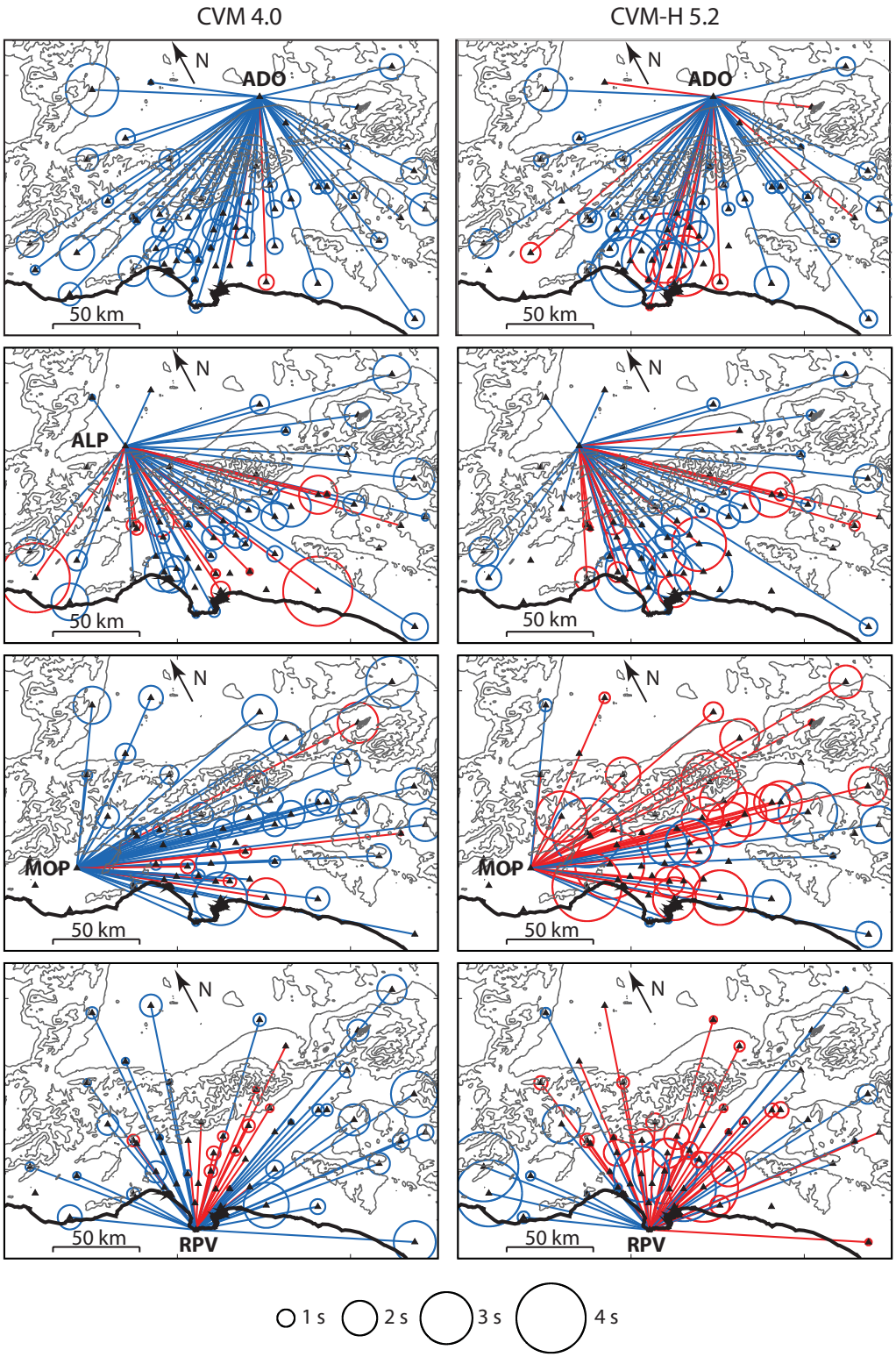

Figure 9. The ray paths and time lags between the ambient-noise and finite-element Green's functions are mapped on the Earth's surface assuming that the virtual source is at station ADO, ALP, MOP, RPV, SDD, and RVR, respectively. Only paths with normalized cross-correlation coefficient above 0.3 and interstation distance greater than 30 km are shown. Ray paths are approximated by straight lines. The negative time lags (ambient-noise arrivals later) are shown in blue and positive time lags (ambient-noise arrivals earlier) are in red. The amplitude of the lags is denoted by the radius of the circle. The scale is shown at the bottom of the figure. (*Continued*)

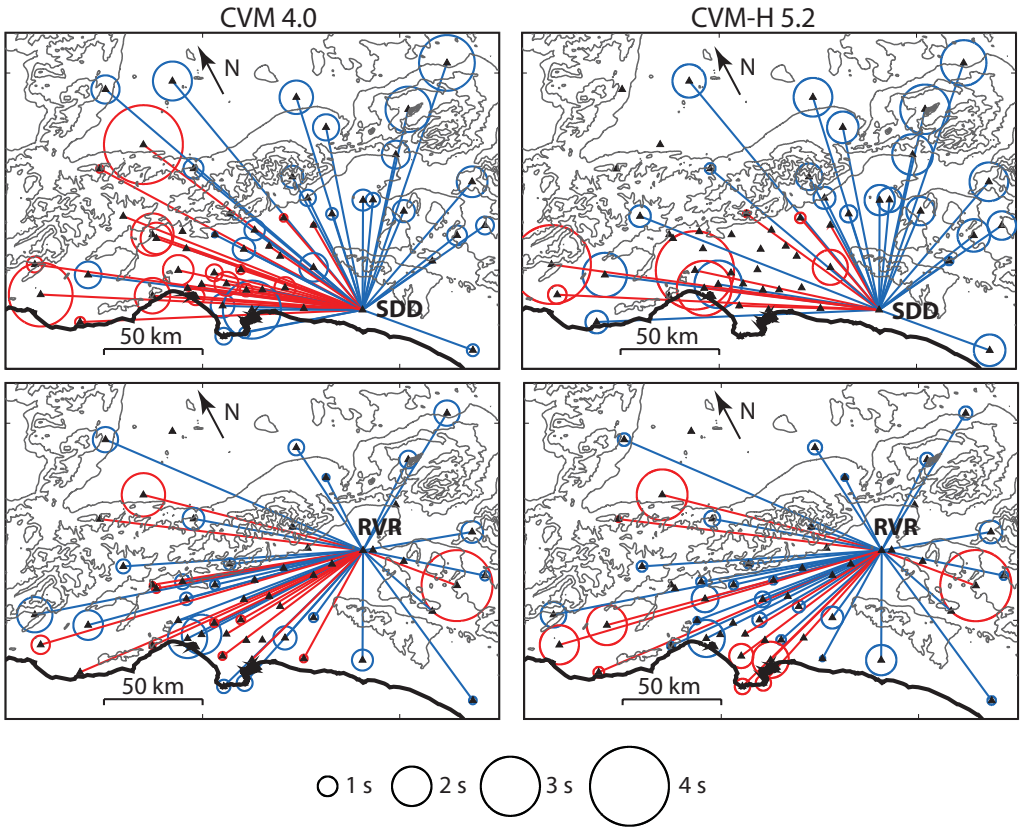

Figure 9. Continued.

the finite-element and ambient-noise solution is largely independent of both interstation distance and azimuth. In CVM 4.0, 73% of paths have a correlation coefficient greater than 0.5, indicating a good correlation, whereas for CVM-H 5.2, only 49% of the ray paths show such a good correlation. 5% of the paths in CVM 4.0 and 22% of the paths in CVM-H 5.2 have a correlation coefficient below 0.3. Of the 295 paths, the mean correlation coefficient is 0.62 for CVM 4.0 and 0.49 for CVM-H 5.2; for 74% of the paths, CVM 4.0 has a larger correlation coefficient. All of these metrics indicate greater waveform similarity between the data and CVM 4.0 than between the data and CVM-H 5.2.

The time lags for ray paths with the correlation coefficient above 0.3 in both community velocity models and the interstation distance larger than 30 km tell a different story (Fig. 11). There are total 225 ray paths. The scatter of time lags in CVM-H 5.2 is larger than in CVM 4.0. Here again, time lag does not vary systematically with the interstation distance or azimuth. In CVM 4.0, 77% of the ray paths show a negative time lag, indicating that CVM 4.0 generates material velocities that are too fast, whereas in CVM-H 5.2, only 61% of the ray paths show a negative time lag. It is worth noting that several time-lag measurements in both CVMs reach the time-lag limit we imposed (−4 and 4 sec). The median time lag is −0.71 sec for CVM 4.0 and −0.42 sec for CVM-H 5.2, suggesting that CVM-H 5.2 does a better job at predicting arrival times than CVM 4.0. If we compare the predictions of the models to each other, we find that for 67% of the ray paths, the time lags in CVM 4.0 are smaller than for CVM-H 5.2, indicating that CVM 4.0 has velocities that are faster than CVM-H 5.2 along the paths we sampled.

Discussion

Our analysis demonstrates the advantage of using ambient noise to test velocity models. Each station acts as a virtual source and the source excitation is known: a unit force applied at the station. Alternative assessments of 3D velocity models are available using the Z/H ratio (Shikato *et al.*, 2007; Yano *et al.*, 2007) of Rayleigh waves or waveform data from small earthquakes (Komatitsch *et al.*, 2004; Rogers *et al.*, 2008). As noted in Rogers *et al.* (2008), the assessment using earthquake data is sensitive to uncertainties in the earthquake source location, origin time, and source time function. Also, earthquakes can be infrequent and their locations cannot be predetermined or controlled; however, an important advantage for earthquake data is that they contain higher frequency energy than the ambient-noise Green's functions.

Derivations of the conditions under which Green's functions will emerge from ambient noise assume an isotropic distribution of the noise sources and/or scatters for the true Green's function to be retrieved—a condition that might not

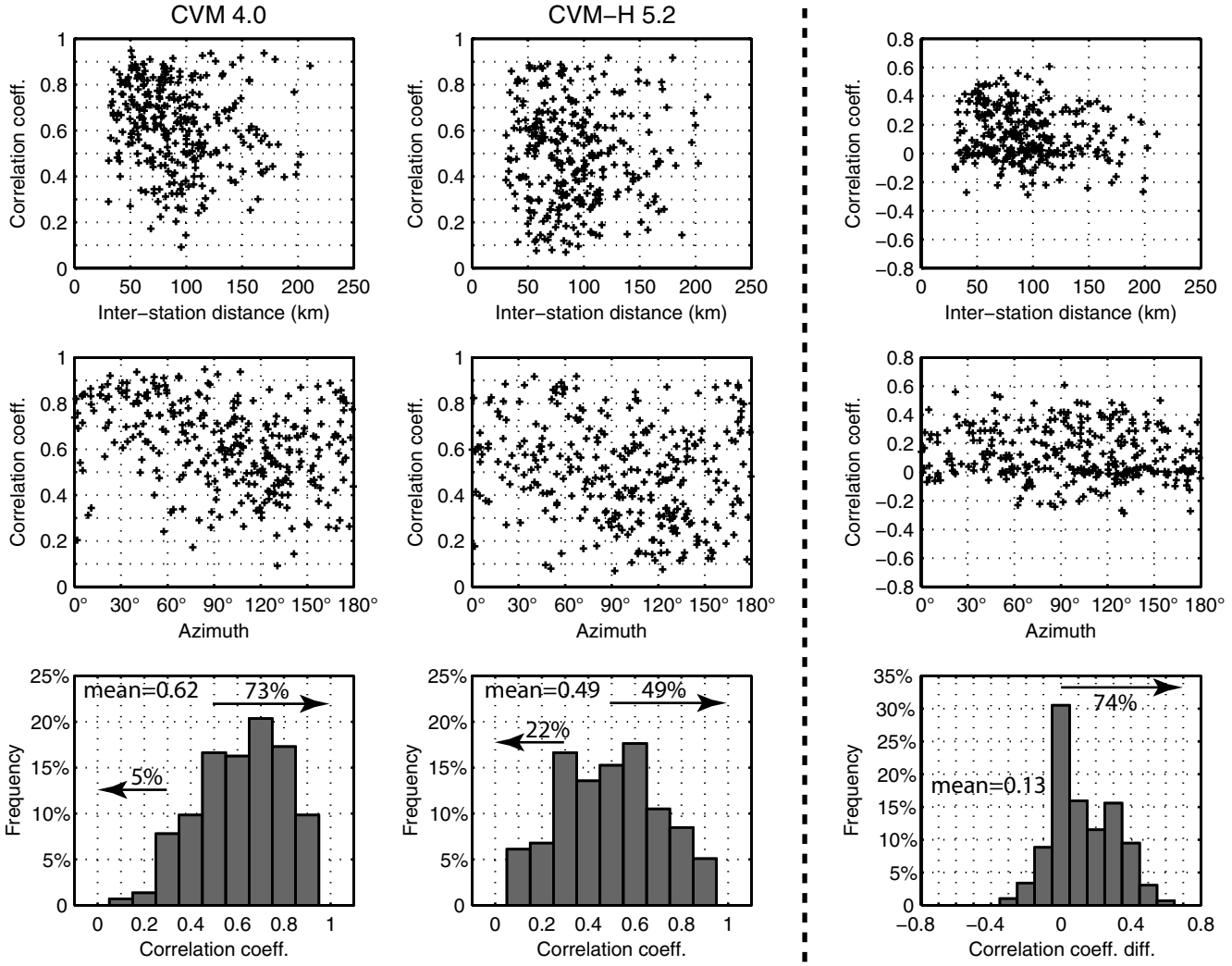

Figure 10. Plot of the correlation coefficient and the correlation coefficient difference between CVM 4.0 and CVM-H 5.2 (correlation coefficient in CVM 4.0 minus that in CVM-H 5.2) as a function of interstation distance and azimuth for all of the station-to-station paths with the interstation distance greater than 30 km and histograms of the correlation coefficient and the correlation coefficient difference. There is a total of 295 paths in each community velocity model. 73% of the ray paths in the CVM 4.0 and 49% of the ray paths in the CVM-H 5.2 have a correlation coefficient above 0.5. 5% of the ray paths in the CVM 4.0 and 22% of the ray paths in the CVM-H 5.2 have a correlation coefficient below 0.3. CVM 4.0 has a larger correlation coefficient than CVM-H 5.2 along 74% of the ray paths. All indicate that CVM 4.0 correlates better with the ambient-noise solution than CVM-H 5.2.

be satisfied in nature. The scattering caused by the small-scale heterogeneities in the crust and the randomization of noise sources when taking very long seismic noises would help us to realize this condition that may still not be realized. The sense of the bias in such measurements would be to increase the velocities. That is, the apparent velocity (phase velocity) for a nongreat circle arrival that might arise from a nonisotropic distribution of noise sources would be higher than the true velocity. The fact that the mean residuals in our results cluster about zero supports the notion that our results are not strongly biased by a nonisotropic recorded wave field. We have shown that the Green's functions are stable over time. Future work may clarify whether and how much the uneven distribution of noise sources might affect the velocity of the surface-wave Green's functions.

Sabra *et al.* (2005a) showed that ambient-noise Green's functions are sensitive to the orientation of station-to-station path with respect to the coast in southern California. The Green's functions for paths that are perpendicular to the coast have a larger SNR than paths that are parallel to the coast. We observe the same effect; however, although the SNR is small, there is enough signal for a reliable measurement (see stations LDR and RDM in Fig. 8a, for example). We find no dependence of correlation coefficient or time lag between the finite-element and ambient-noise waveforms on the interstation distance or azimuth.

Although the original noise time series has energy between 0.01 and 5 Hz, the Green's functions obtained from correlation have a dominant frequency band of 0.1–0.2 Hz for most paths, which is controlled by the frequency band

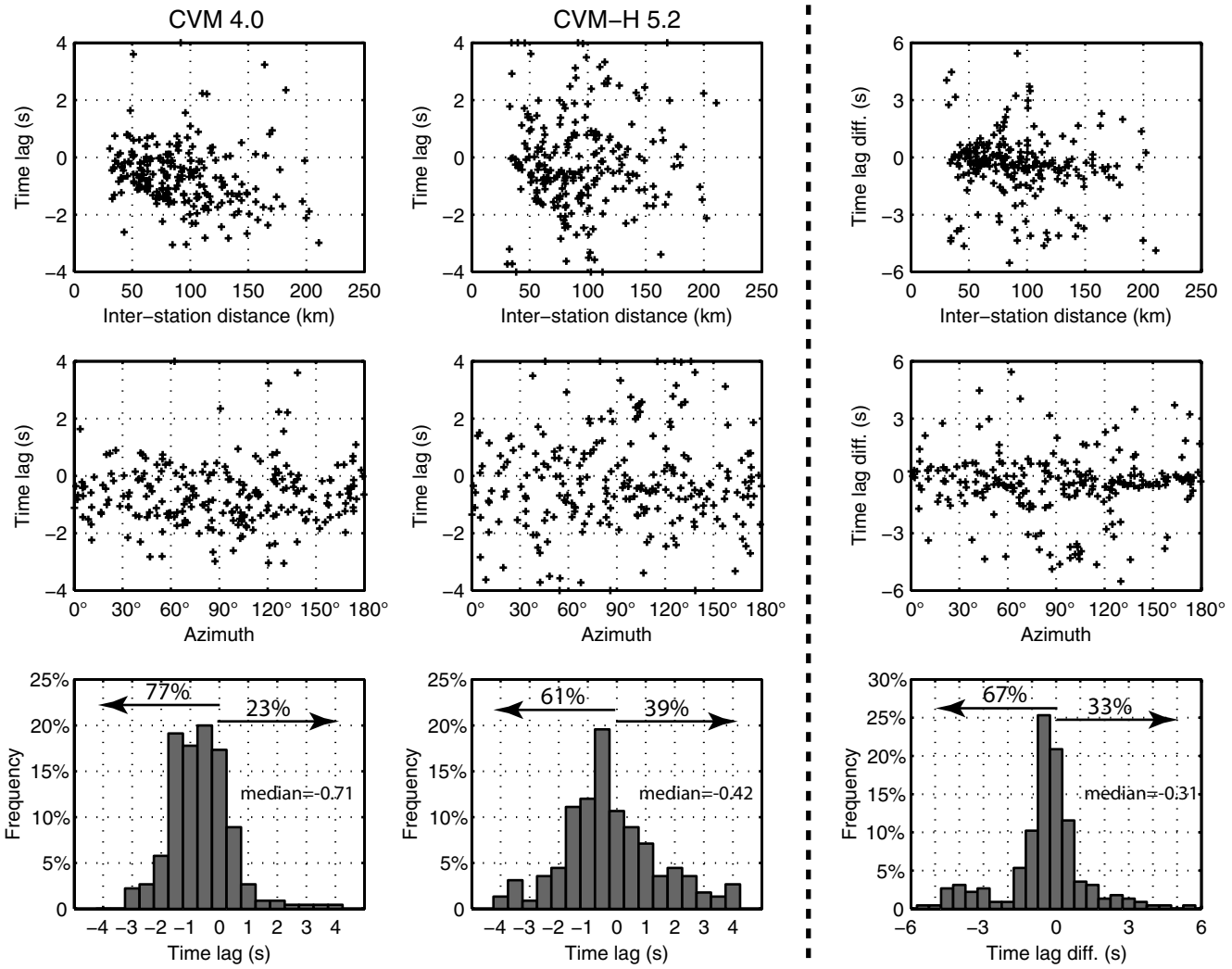

Figure 11. Plot of the time lag and the time-lag difference between CVM 4.0 and CVM-H 5.2 (time lag in CVM 4.0 minus that in CVM-H 5.2) as a function of interstation distance and azimuth for all of the station-to-station paths and histograms of the time lag and the time-lag difference between CVM 4.0 and CVM-H 5.2. Only ray paths with the normalized correlation coefficient above 0.3 in both community models and the interstation distance greater than 30 km are shown. There is a total of 225 paths. 77% of the ray paths in CVM 4.0 and 61% of the ray paths in CVM-H 5.2 show that the community velocity model is too fast. CVM 4.0 is faster than CVM-H 5.2 along 67% of the paths.

of microseisms (Aki and Richards, 1980). These long-period Green's functions are most sensitive to the velocity structure in the upper 10 km of the crust. The minimum shear-wave velocity limit (500 m/sec) we impose for the near-surface sediments in the finite-element simulations should have a minimal effect on our results. Pushing the ambient-noise Green's function to higher frequencies will place stronger constraints on the velocity models, and it is an important research frontier; however, it is likely to be challenging to extract coherent wave fields at increasingly higher frequencies.

We note that complex waveforms of either the finite-element or ambient-noise results can affect our estimate of time lag and correlation coefficient between them. For example, for the station pair (RPV-WLT, Fig. 8d), the correlation coefficient between the finite-element waveforms in the CVM 4.0 is 0.75; however, it decreases to 0.37 in the CVM-H 5.2. This is largely due to the late reverberations in the CVM-H 5.2 time series. The finite-element waveforms in the CVM-H 5.2 tend to have more reverberations in the later part of time series than those in the CVM 4.0 in most of the comparisons, which is probably due to the slower and/or more heterogeneous material velocities in the CVM-H 5.2 in the sedimentary basins. This may explain why the CVM-H 5.2 has a lower waveform similarity with the ambient-noise results. It is conceivable that seismic attenuation would dampen the late reverberations to some extent; however, at this stage we prefer to avoid the temptation of introducing an adjustable parameter.

The time lags we found are defined along the whole length of each ray path. Therefore, it does not constrain directly where the community velocity models might be fast or slow. The time-lag data in our analysis can be used directly in

seismic tomography, and because they will include finite-frequency effects, they are particularly suitable for input to the adjoint method (Tromp *et al.*, 2005; Liu and Tromp, 2006) or the scattering-integral formulation (Chen *et al.*, 2007) to develop improved community velocity models.

Conclusions

By correlating monthly ambient seismic noise data recorded at 56 broadband seismic stations in southern California, we determine station-to-station Green's functions. These Green's functions provide an independent and important test of the current SCEC community velocity models (CVM 4.0 and CVM-H 5.2).

Ambient-noise Green's functions and theoretical Green's functions, calculated using the finite-element method of Ma and Liu (2006) in the CVM 4.0 and CVM-H 5.2, for nearly 300 paths with a good azimuthal coverage of the Los Angles Basin, show strong waveform similarity in the dominant surface waves between 0.1 and 0.2 Hz. The CVM 4.0 predictions have stronger waveform similarity with the ambient-noise Green's functions than those from CVM-H 5.2. On the other hand, CVM-H 5.2 does a better job at predicting arrival times. Measurements obtained from the ambient-noise approach can be used directly for refinement of community velocity models. Moreover, the ambient-noise approach will allow us to control the location of virtual sources that can be arranged to target parts of the velocity models that are poorly constrained or areas of critical importance for seismic hazard analysis.

Data and Resources

Data used in this study can be obtained from the Southern California Earthquake Data Center at www.data.scec.org.

Acknowledgments

We thank two anonymous reviewers and Arben Pitarka (Associate Editor) for constructive comments, and Andreas Plesch and Harold Magistrale for their help on the use of SCEC community velocity models. This work is supported by the SCEC, which is funded by the National Science Foundation (NSF) Cooperative Agreement EAR-0106924 and the U.S. Geological Survey (USGS) Cooperative Agreement 02HQAG0008. The Center for Computational Earth and Environmental Sciences at Stanford University provided the computational resources for all the simulations. This is SCEC contribution number 1211.

References

Aki, K. (1957). Space and time spectra of stationary stochastic waves with special reference to microtremors, *Bull. Earthquake Res. Inst. Tokyo Univ.* **35,** 415–456.

Aki, K., and B. Chouet (1975). Origin of coda waves: source, attenuation and scattering effects, *J. Geophys. Res.* **80,** 3322–3342.

Aki, K., and P. G. Richards (1980). *Quantitative Seismology*, W. H. Freeman and Company, San Francisco.

Bensen, G. D., M. H. Ritzwoller, and N. M. Shapiro (2008). Broadband ambient noise surface wave tomography across the United States, *J. Geophys. Res.* **113,** B05305, doi 10.1029/2007JB005248.

Bensen, G. D., M. H. Ritzwoller, M. P. Barmin, A. L. Levshin, F. Lin, M. P. Moschetti, N. M. Shapiro, and Y. Yang (2007). Processing seismic ambient noise data to obtain reliable broad-band surface wave dispersion measurements, *Geophys. J. Int.* **169,** 1239–1260.

Brenguier, F., N. M. Shapiro, M. Campillo, A. Nercessian, and V. Ferrazzini (2007). 3-D surface wave tomography of the Piton de la Fournaise volcano using seismic noise correlations, *Geophys. Res. Lett.* **34,** L02305, doi 10.1029/2006GL028586.

Brenguier, F., N. M. Shapiro, M. Campillo, V. Ferrazzini, Z. Duputel, O. Coutant, and A. Nercessian (2008). Towards forecasting volcanic eruptions using seismic noise, *Nature Geosci.* **1,** 126–130, doi 10.1038/ngeo104.

Campillo, M. (2006). Phase and correlation in 'random' seismic fields and the reconstruction of the Green function, *Pure Appl. Geophys.* **163,** 475–502.

Campillo, M., and A. Paul (2003). Long range correlations in the seismic coda, *Science* **299,** 547–549.

Chen, P., L. Zhao, and T. H. Jordan (2007). Full 3D tomography for the crustal structure of the Los Angeles region, *Bull. Seismol. Soc. Am.* **97,** 1094–1120, doi 10.1785/0120060222.

Cho, K. H., R. B. Herrmann, C. J. Ammon, and K. Lee (2007). Imaging the upper crust of the Korean Peninsula by surface-wave tomography, *Bull. Seismol. Soc. Am.* **97,** no. 1B, 198–207.

Claerbout, J. F. (1968). Synthesis of a layered medium from its acoustic transmission response, *Geophysics* **33,** 264–269.

de Hoop, A. T. (1960). A modification of Cagniard's method for solving seismic pulse problems, *Appl. Sci. Res.* **B8,** 349–356.

Derode, A., E. Larose, M. Tanter, J. de Rosny, A. Tourin, M. Campillo, and M. Fink (2003). Recovering the Green's function from field-field correlations in an open scattering medium (*L*), *J. Acoust. Soc. Am.* **113,** 2973–2976.

Duvall, T. L., S. M. Jefferies, J. W. Harvey, and M. A. Pomerantz (1993). Time distance helioseismology, *Nature* **362,** 430–432.

Gerstoft, P., K. Sabra, P. Roux, W. Kuperman, and M. Fehler (2006). Green's functions extraction and surface-wave tomography from microseisms in southern California, *Geophysics* **71,** no. 4, 23–31.

Graves, R. W. (1998). Three-dimensional finite-difference modeling of the San Andreas fault: source parameterization and ground-motion levels, *Bull. Seismol. Soc. Am.* **88,** 881–897.

Hauksson, E. (2000). Crustal structure and seismicity distribution adjacent to the Pacific and North America plate boundary in southern California, *J. Geophys. Res.* **105,** 13,875–13,903.

Kohler, M. D., H. Magistrale, and R. W. Clayton (2003). Mantle heterogeneities and the SCEC reference three-dimensional seismic velocity model, version 3, *Bull. Seismol. Soc. Am.* **93,** 757–774.

Komatitsch, D., Q. Liu, J. Tromp, P. Süss, C. Stidham, and J. H. Shaw (2004). Simulation of ground motion in the Los Angeles basin based upon the spectral-element method, *Bull. Seismol. Soc. Am.* **94,** 187–206.

Lamb, H. (1904). On the propagation of tremors over the surface of an elastic solid, *Phil. Trans. R. Soc. London A* **203,** 1–42.

Larose, E., A. Derode, M. Campillo, and M. Fink(2004). Imaging from one-bit correlations of wideband diffuse wavefields, *J. Acoust. Soc. Am.* **95,** 8393–8399.

Larose, E., A. Khan, Y. Nakamura, and M. Campillo (2005). Lunar subsurface investigated from correlation of seismic noise, *Geophys. Res. Lett.* **32,** L16201, doi 10.1029/2005GL023518.

Liang, C., and C. A. Langston (2008). Ambient seismic noise tomography and structure of eastern North America, *J. Geophys. Res.* **113,** B03309, doi 10.1029/2007JB005350.

Lin, F., M. P. Moschetti, and M. H. Ritzwoller (2008). Surface wave tomography of the western United States from ambient seismic noise: Rayleigh and Love wave phase velocity maps, *Geophys. J. Int.* **173,** 281–298, doi 10.1111/j.1365-246X.2008.03720.x.

Lin, F., M. H. Ritzwoller, J. Townend, M. Savage, and S. Bannister (2007). Ambient noise Rayleigh wave tomography of New Zealand, *Geophys. J. Int.* **170,** no. 2, 649–666, doi 10.1111/j.1365-246X.2007.03414.x.

Liu, Q., and J. Tromp (2006). Finite-frequency kernels based upon adjoint methods, *Bull. Seismol. Soc. Am.* **96,** 2383–2397.

Lobkis, O. I., and R. L. Weaver (2001). On the emergence of the Green's function in the correlations of a diffuse field, *J. Acoust. Soc. Am.* **110,** 3011–3017.

Ma, S., and P. Liu (2006). Modeling of the perfectly matched layer absorbing boundaries and intrinsic attenuation in explicit finite-element methods, *Bull. Seismol. Soc. Am.* **96,** 1779–1794, doi 10.1785/0120050219.

Ma, S., R. J. Archuleta, and M. T. Page (2007). Effects of large-scale surface topography on ground motions, as demonstrated by a study of the San Gabriel Mountains, Los Angeles, California, *Bull. Seismol. Soc. Am.* **97,** 2066–2079, doi 10.1785/0120070040.

Magistrale, H., S. Day, R. W. Clayton, and R. Graves (2000). The SCEC Southern California reference three-dimensional seismic velocity model version 2, *Bull. Seismol. Soc. Am.* **90,** S65–S76.

Malcolm, A. E., J. A. Scales, and B. A. van Tiggelen (2004). Extracting the Green function from diffuse, equipartitioned waves, *Phys. Rev. E* **70,** 015601, doi 10.1103/PhysRevE.70.015601.

Moschetti, M. P., M. H. Ritzwoller, and N. M. Shapiro (2007). Surface wave tomography of the western United States from ambient seismic noise: Rayleigh wave group velocity maps, *Geochem. Geophys. Geosyst.* **8,** Q08010, doi 10.1029/2007GC001655.

Olsen, K. B., R. J. Archuleta, and J. R. Matarese (1995). Three-dimensional simulation of a magnitude 7.75 earthquake on the San Andreas fault, *Science* **270,** 1628–1632.

Olsen, K. B., S. M. Day, J. B. Minster, Y. Cui, A. Chourasia, M. Faerman, R. Moore, P. Maechling, and T. Jordan (2006). Strong shaking in Los Angeles expected from southern San Andreas earthquake, *Geophys. Res. Lett.* **33,** L07305, doi 10.1029/2005GL025472.

Paul, A., M. Campillo, L. Margerin, E. Larose, and A. Derode (2005). Empirical synthesis of time-asymmetrical Green functions from the correlation of coda waves, *J. Geophys. Res.* **110,** B08302, doi 10.1029/2004JB003521.

Prieto, G., and G. C. Beroza (2008). Earthquake ground motion prediction using ambient seismic field, *Geophys. Res. Lett.* **35,** L14304, doi 10.1029/2008GL034428.

Rickett, J., and J. Claerbout (1999). Acoustic daylight imaging via spectral factorization: helioseismology and reservoir monitoring, *Leading Edge* **18,** 957–960.

Rodgers, A., N. A. Petersson, S. Nilsson, B. Sjogreen, and K. McCandless (2008). Broadband waveform modeling of moderate earthquakes in the San Francisco by area and preliminary assessment of the USGS 3D seismic velocity model, *Bull. Seismol. Soc. Am.* **98,** 969–988, doi 10.1785/0120060407.

Roux, P., and W. A. KupermanNPAL Group (2004). Extracting coherent wavefronts from acoustic ambient noise in the ocean, *J. Acoust. Soc. Am.* **116,** 1995–2003.

Roux, P., K. G. Sabra, W. A. Kuperman, and A. Roux (2005). Ambient noise cross correlation in free space: theoretical approach, *J. Acoust. Soc. Am.* **117,** 79–84.

Sabra, K. G., P. Roux, and W. A. Kuperman (2005). Arrival-time structure of the time-averaged ambient noise cross-correlation function in an oceanic waveguide, *J. Acoust. Soc. Am.* **117,** 164–174.

Sabra, K. G., P. Gerstoft, P. Roux, W. A. Kuperman, and M. C. Fehler (2005a). Extracting time-domain Green's function estimates from ambient seismic noise, *Geophys. Res. Lett.* **32,** L03310, doi 10.1029/2004GL021862.

Sabra, K. G., P. Gerstoft, P. Roux, W. A. Kuperman, and M. C. Fehler (2005b). Surface wave tomography from microseisms in southern California, *Geophys. Res. Lett.* **32,** L14311, doi 10.1029/2005GL023155.

Sánchez-Sesma, R. J., and M. Campillo (2006). Retrieval of the Green's function from cross correlation: the canonical elastic problem, *Bull. Seismol. Soc. Am.* **96,** 1182–1191, doi 10.1785/0120050181.

Sánchez-Sesma, R. J., J. A. Pérez-Ruiz, M. Campillo, and F. Luzón (2006). Elastodynamic 2D Green function retrieval from cross-correlation: canonical inclusion problem, *Geophys. Res. Lett.* **33,** L13305, doi 10.1029/2006GL026454.

Sato, H., and M. Fehler (1998). *Wave Propagation and Scattering in the Heterogeneous Earth*, Springer-Verlag, Berlin.

Shapiro, N. M., and M. Campillo (2004). Emergence of broadband Rayleigh waves from correlations of the ambient seismic noise, *Geophys. Res. Lett.* **31,** L07614, doi 10.1029/2004GL019491.

Shapiro, N. M., M. Campillo, L. Stehly, and M. Ritzwoller (2005). High resolution surface wave tomography from ambient seismic noise, *Science* **307,** 1615–1618.

Shikato, S., T. Yano, and T. Tanimoto (2007). The *ZH* ratio analysis of Rayleigh waves using broadband seismograms in southern California (Abstract S41A-0251), *Eos Trans. AGU* **88,** no. 52, (Fall Meet. Suppl.), S41A-0251.

Snieder, R. (2004). Extracting the Green's function from the correlation of coda waves: a derivation based on stationary phase, *Phys. Rev. E* **69,** 046610.

Snieder, R., K. Wapenaar, and U. Wegler (2007). Unified Green's function retrieval by cross-correlation; connection with energy principles, *Phys. Rev. E* **75,** 036103.

Süss, M. P., and J. H. Shaw (2003). *P*-wave seismic velocity structure derived from sonic logs and industry reflection data in the Los Angeles basin, California, *J. Geophys. Res.* **108,** no. B3, 2170, doi 10.1029/2001JB001628.

Tromp, J., C. Tape, and Q. Liu (2005). Seismic tomography, adjoint methods, time reversal, and banana-donut kernels, *Geophys. J. Int.* **160,** 195–216, doi 10.1111/j.1365-246X.2004.02453.x.

Wapenaar, K. (2004). Retrieving the elastodynamic Green's function of an arbitrary inhomogeneous medium by cross correlation, *Phys. Rev. Lett.* **93,** 254301-1–4.

Weaver, R. L., and O. I. Lobkis (2001). Ultrasonics without a source: thermal fluctuation correlations at MHz frequencies, *Phys. Rev. Lett.* **87,** 134301-1–4.

Weaver, R. L., and O. I. Lobkis (2004). Diffuse fields in open systems and the emergence of the Green's function, *J. Acoust. Soc. Am.* **116,** 2731–2734.

Wegler, U., and C. Sens-Schönfelder (2007). Fault zone monitoring with passive image interferometry, *Geophys. J. Int.* **168,** 1029–1033.

Yang, Y., A. Li, and M. H. Ritzwoller (2008). Crustal and uppermost mantle structure in southern Africa revealed from ambient noise and teleseismic tomography, *Geophys. J. Int.* **174,** 235–248, doi 10.1111/j.1365-246X.2008.03779.x.

Yang, Y., M. H. Ritzwoller, A. L. Levshin, and N. M. Shapiro (2007). Ambient noise Rayleigh wave tomography across Europe, *Geophys. J. Int.* **168,** no. 1, 259–274.

Yano, T., S. Shikato, L. Rivera, and T. Tanimoto (2007). The *ZH* ratio analysis of global seismic data (Abstract S41A-0251), *Eos Trans. AGU* **88,** no. 52, (Fall Meet. Suppl.), S41A-0251.

Yao, H., C. Beghein, and R. D. van der Hilst (2008). Surface wave array tomography in SE Tibet from ambient seismic noise and two-station analysis—II. crustal and upper-mantle structure, *Geophys. J. Int.* **173,** 205–219.

Yao, H., R. D. van der Hilst, and M. V. de Hoop (2006). Surface-wave array tomography in SE Tibet from ambient seismic noise and two-station analysis—I. phase velocity maps, *Geophys. J. Int.* **166,** no. 2, 732–744.

Zheng, S., X. Sun, X. Song, Y. Yang, and M. H. Ritzwoller (2008). Surface wave tomography of China from ambient seismic noise correlation, *Geochem. Geophys. Geosyst.* **9,** Q05020, doi 10.1029/2008GC001981.

Department of Geophysics
Stanford University
397 Panama Mall
Stanford, California 94305

Manuscript received 23 August 2008